AWARD NUMBER: W81XWH-15-C-0125

TITLE: A Modular Multi-DOF Prosthetic Wrist and Low-Level Autonomous Control for Ease-of-Use

PRINCIPAL INVESTIGATOR: Aaron Dollar

CONTRACTING ORGANIZATION: Yale University, New Haven, CT

REPORT DATE: June 2021

TYPE OF REPORT: Final

PREPARED FOR: U.S. Army Medical Research and Development Command
Fort Detrick, Maryland 21702-5012

REPORT DOCUMENTATION PAGE

Form Approved
OMB No. 0704-0188

1. REPORT DATE	**2. REPORT TYPE**	**3. DATES COVERED**
June 2021	Final	**30Sep2015-29Jun2021**

4. TITLE AND SUBTITLE

A Modular Multi-DOF Prosthetic Wrist and Low-Level Autonomous Control for Ease of Use

5a. CONTRACT NUMBER
W81XWH-15-C-0125

5b. GRANT NUMBER

5c. PROGRAM ELEMENT NUMBER

6. AUTHOR(S)

Aaron Dollar, Linda Resnik, He Huang

E-Mail:

5d. PROJECT NUMBER

5e. TASK NUMBER

5f. WORK UNIT NUMBER

7. PERFORMING ORGANIZATION NAME(S) AND ADDRESS(ES)
Yale University, New Haven, CT 06511

8. PERFORMING ORGANIZATION REPORT NUMBER

9. SPONSORING / MONITORING AGENCY NAME(S) AND ADDRESS(ES)

U.S. Army Medical Research and Development Command
Fort Detrick, Maryland 21702-5012

10. SPONSOR/MONITOR'S ACRONYM(S)

11. SPONSOR/MONITOR'S REPORT NUMBER(S)

12. DISTRIBUTION / AVAILABILITY STATEMENT

Approved for Public Release; Distribution Unlimited

13. SUPPLEMENTARY NOTES

14. ABSTRACT

The proposed project centers on developing and evaluating a novel class of spherical prosthetic wrist that provides a range of motion equal to the unaffected human wrist while adding only two inches to the length of the residual limb. This device will be enabled by an intuitive pattern recognition-based surface electromyography (EMG) control scheme to directly control the three degrees of freedom of the wrist and one degree of freedom of the user's terminal device, as well as smart low-level autonomy to enable functions such as "autolevel" to reduce cognitive loads for tasks such as keeping a soup spoon level during eating.

15. SUBJECT TERMS
Upper Limb Prosthetics, Amputee, Assistive Technology, Motion Capture

16. SECURITY CLASSIFICATION OF:			**17. LIMITATION OF ABSTRACT**	18. NUMBER OF PAGES	**19a. NAME OF RESPONSIBLE PERSON**
a. REPORT	**b. ABSTRACT**	**c. THIS PAGE**			USAMRMC
Unclassified	Unclassified	Unclassified	Unclassified	52	**19b. TELEPHONE NUMBER** *(include area code)*

Contents

1. INTRODUCTION

The proposed project centers on developing and evaluating a novel class of spherical prosthetic wrist that provides a range of motion equal to the unaffected human wrist while adding only two inches to the length of the residual limb. This device will be enabled by an intuitive pattern recognition-based surface electromyography (EMG) control scheme to directly control the three degrees of freedom of the wrist and one degree of freedom of the user's terminal device, as well as smart low-level autonomy to enable functions such as "autolevel" to reduce cognitive loads for tasks such as keeping a soup spoon level during eating. These concepts will be tested through both a participatory research plan involving amputee end-user from conception, refinement to preliminary testing, as well as a six-subject amputee pilot study in the final year, conducted at the VA New York Harbor Health Care System (Manhattan).

2. KEYWORDS

Upper Limb Prosthetics, Amputee, Assistive Technology, Motion Capture

3. ACCOMPLISHMENTS

This document covers the final report of the project.

3.1 What were the major goals of the project?

The major goals of this project are to develop a novel 3 degree-of-freedom (DOF) prosthetic wrist and associated pattern recognition based myoelectric (surface EMG) control scheme. This scheme will simplify the challenges associated with controlling multiple DOF simultaneously, from limited control sites on the residual limb. The scheme will also grant the user access to semi-autonomous 'smart control modes. These modes involved such functions as keep a soup spoon level while eating or taking care of some of the wrist motion that exists when bringing a cup to one's mouth for drinking.

The technical components and smart control concepts were tested and iteratively developed via able bodied participants via a number of sub studies to be carried out at both Yale and NCSU.

3.2 What was accomplished under these goals?

All teams combined efforts for project planning, leading to the following achievements.

Yale Hardware Group Accomplishments

Year 1

The group at Yale carried out initial design work for the prosthetic wrist device. In particular, the following achievements have been made:

1. A parallel mechanism design topology was proposed after previously surveying the current field of wrist prostheses
2. An initial CAD model was created for motion simulation and verification (Figure 1)
3. The design was optimized based on range of motion requirements
    a. Forward and inverse kinematics solvers were generated to simulate the full workspace of the prosthesis
    b. Kinematic design parameters were varied to determine their effects on the overall range of motion.
4. The hardware requirements for a realizable prototype were identified (e.g. range of motion for components within the mechanism, actuator stroke requirements, etc.)

5. A new conceptual universal joint design was developed for push-rod integration, based on the geometric requirements of the wrist design (Figure 2).
6. The geometric model of the prosthesis body was refined based on ideal packaging goals.

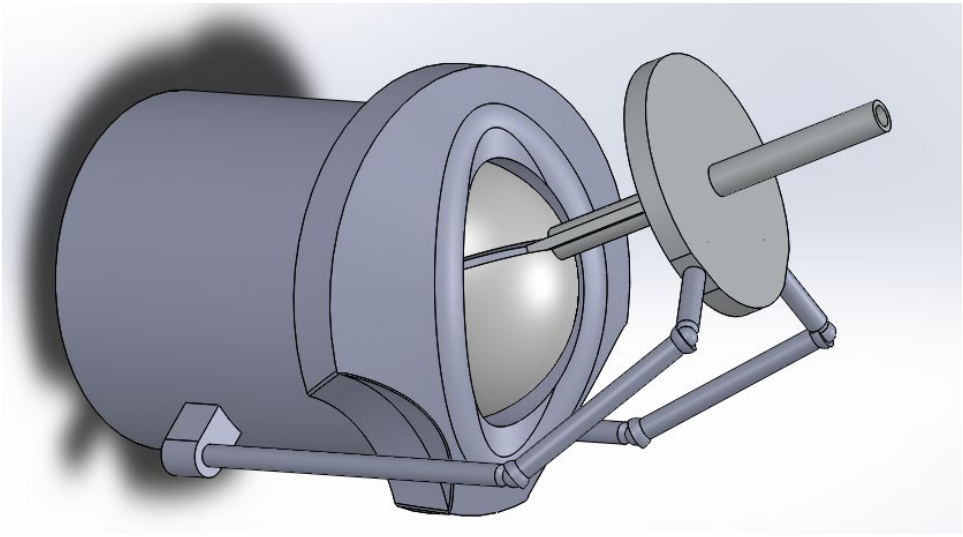

Figure 1. CAD model of the current wrist design, utilizing linear actuators, pushrods and a constrained spherical joint.

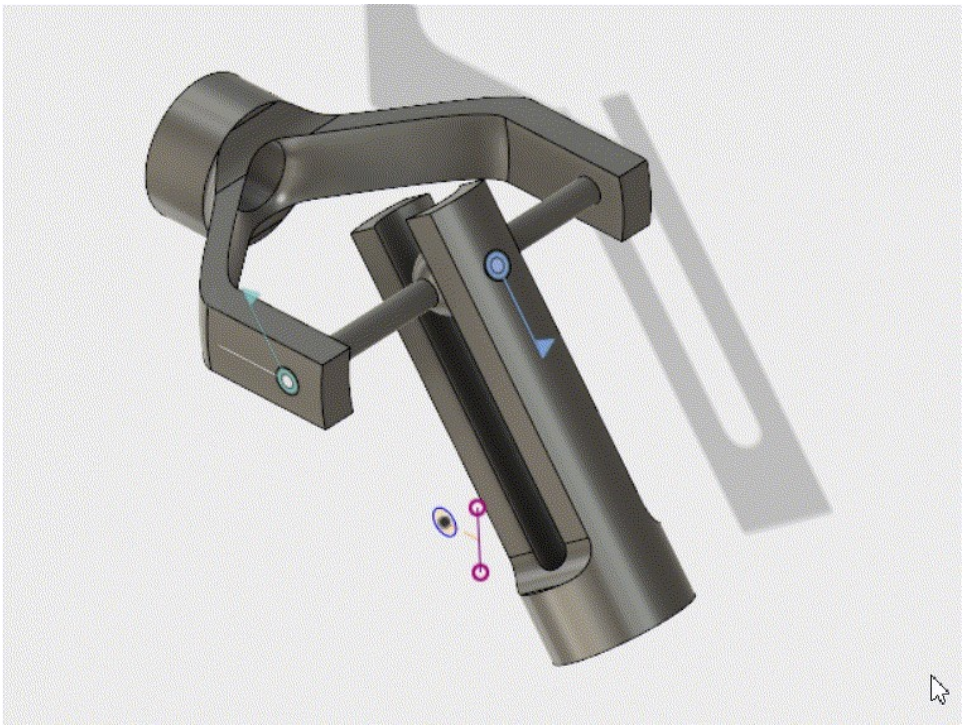

Figure 2. Universal joint geometry required to achieve large angular range of motion at the pushrods joints (the joints are shown in the bottom right region of Figure 1).

Year 2

The group at Yale carried out design optimization and fabrication for the prosthetic wrist device and a paired single actuator prosthetic hand. The following achievements have been made:

1. A 2-DOF submodule (Figure 3 left) of the 3-DOF prosthetic wrist was specified
    a. The geometric design was optimized to generate the best motion characteristics across the desired range of motion. Optimized geometric model can be seen in (Figure 3 right).
    b. Parallel mechanism architecture which imparts flexion/extension and radial/ulnar deviation.
    c. This optimization work was presented at the Myoelectric Controls Symposium 2017.

2. A rudimentary scaled-up prototype of the 2-DOF submodule was developed (Figure 4).

a. All the geometric parameters are adjustable in this prototype.
b. Physically changed design parameters to identify potential issues with regarding parameters and effect on motion quality.

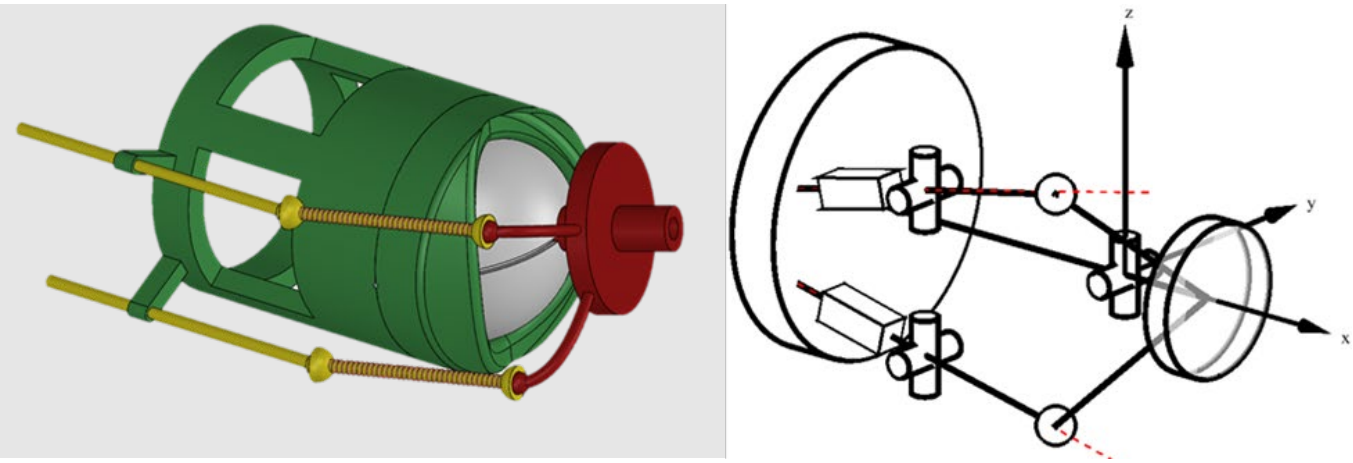

Figure 3. (Left) Schematic of 2-DOF flexion and deviation submodule. Yellow represents the pushrod linear actuators. Red represents the platform on which a terminal device would be attached. (Right) Optimized geometry for the 2-DOF submodule, showing the kinematic configuration and geometric design of the optimized submodule.

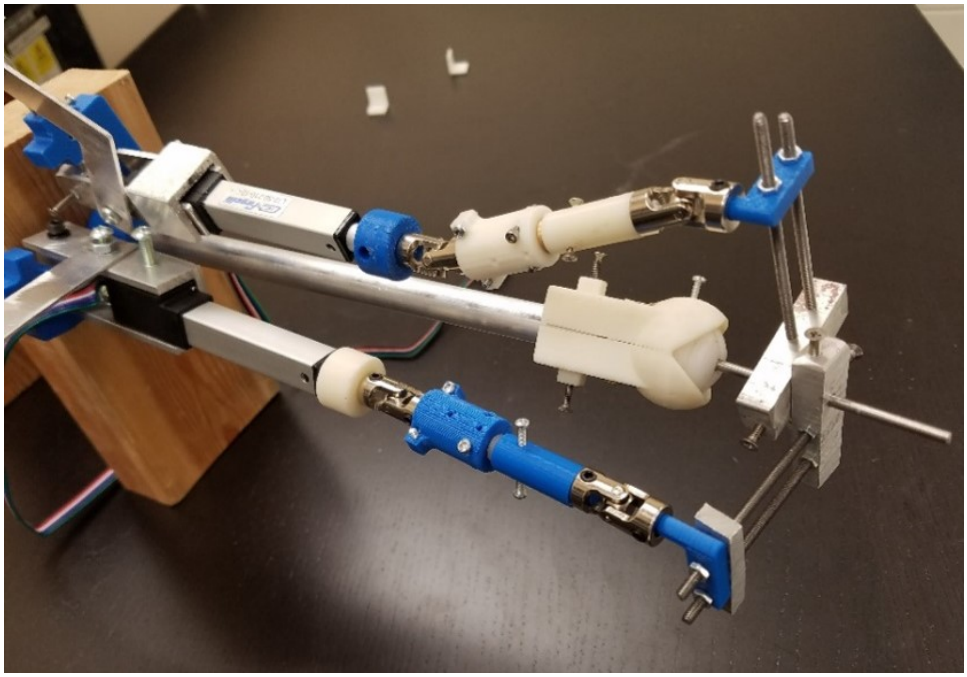

Figure 4. Adjustable parameter prototype of the 2-DOF submodule.

3. A 3-DOF wrist module was also developed based on the insights gained from the 2-DOF submodule (Figure 5 left).
    a. 3-DOF mechanism employs a hybrid mechanism composed of a similar 2-DOF submodule controlling flexion and radial deviation, and a single DOF rotator that controls pronation.
        i. The parallel mechanism is decoupled, meaning that it may be further divided into two separate mechanisms.
    b. An optimization which leveraged the decoupling was carried out over the geometric parameters of this mechanism to maximize the quality of motion over the desired range of motion for the 2-DOF parallel mechanism portion.
        i. The optimized kinematic design may be seen in (Figure 5 right).
    c. A paper regarding the optimization of this mechanism was submitted to the International Conference on Robotics and Automation (ICRA 17).
        i. Pending editorial decision.

d. A passive prototype of an unoptimized version was developed to assess potential limitations or issues that would not be clear from the geometric optimization.

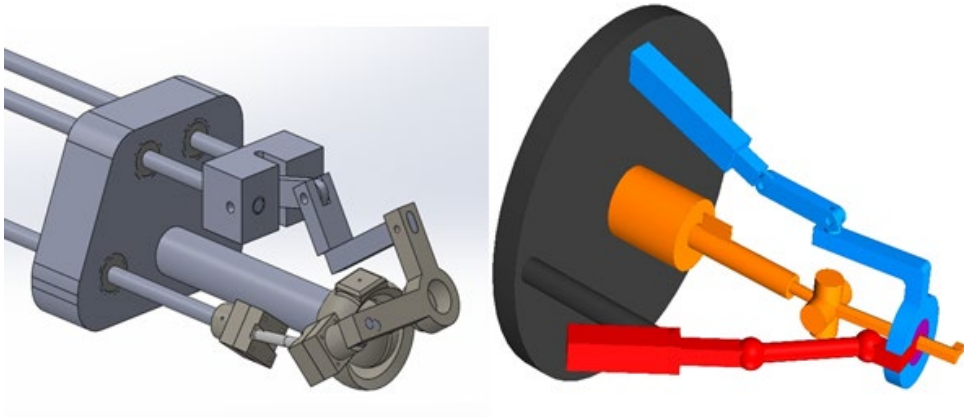

Figure 5. (Left) Model version of the 3-DOF wrist mechanism. (Right) Optimized version of the 3-DOF wrist mechanism. Note the separate sub-mechanisms are shown in different colors: flexion mechanism in blue, deviation mechanism in red, and pronation mechanism in gold.

4. A single actuator anthropomorphic prosthetic hand was created, tested and optimized to be used in conjunction with the multiple degree of freedom wrist. (Figure 6)

    a. The hand has three distinct grasp types which are power or wrap grasp, tripod grasp and lateral grasp.
    b. The hand was revised and optimized for improved force production and performance on activities of daily living.

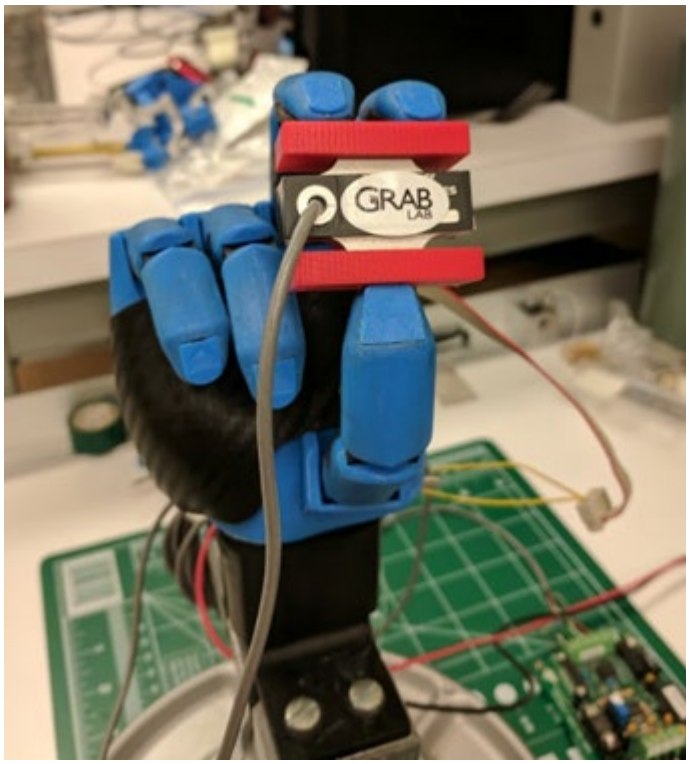

Figure 6. Single actuator underactuated myoelectric hand displaying the tripod grasp which is one of the three grasp types the hand is capable of; this includes power, tripod and lateral grasps.

Year 3

The group at Yale carried out initial design work for the prosthetic **wrist device.** In particular, the following achievements have been made:

We began development of a 3 DOF wrist prototype that a test subject will be able to wear on a bypass socket or be able to be tested as a standalone device.

1. A new methodology for selecting geometric parameters of a parallel mechanism was developed. This methodology is applicable when overall size and clearance of moving parts is critical for the operation of a physical prototype, though hard limits on clearance and size cannot be meaningfully established. This methodology looks at the relative tradeoff between motion performance, clearance, and total size, and how much they may be exchanged for one another.

2. An actuated 3-DOF standalone wrist prototype was developed (Figure 7). The device has an overall length of 18cm, radius of 4.5cm, and a total mass of 578g. Theoretical torque production was calculated and found to be about 10% of maximal human wrist torque in any direction, which is high enough to be useful for manipulation. The speed of the device was tested and found to be comparable to existing commercially available wrist prostheses (Figure 8).

3. A novel redundant spherical joint design was implemented to increase the robustness of this prototype. This spherical joint has high range of motion and significantly more capture area than traditional ball and socket joints, which results in high force capacity. The articular surface geometry has been designed to prevent the joint from becoming immobile in certain positions where the output shaft of the ball contacts the walls of the socket. Algorithms dictating the design and size of these joints have also been developed. This joint design will be relevant to other parallel mechanism designs in addition to this wrist prosthesis.

4. The wrist design has been updated to allow for a socket to be within the unoccupied interior of the wrist (Figure 10). Design work on this wrist continues to minimize the overall length, weight, and complexity of design.

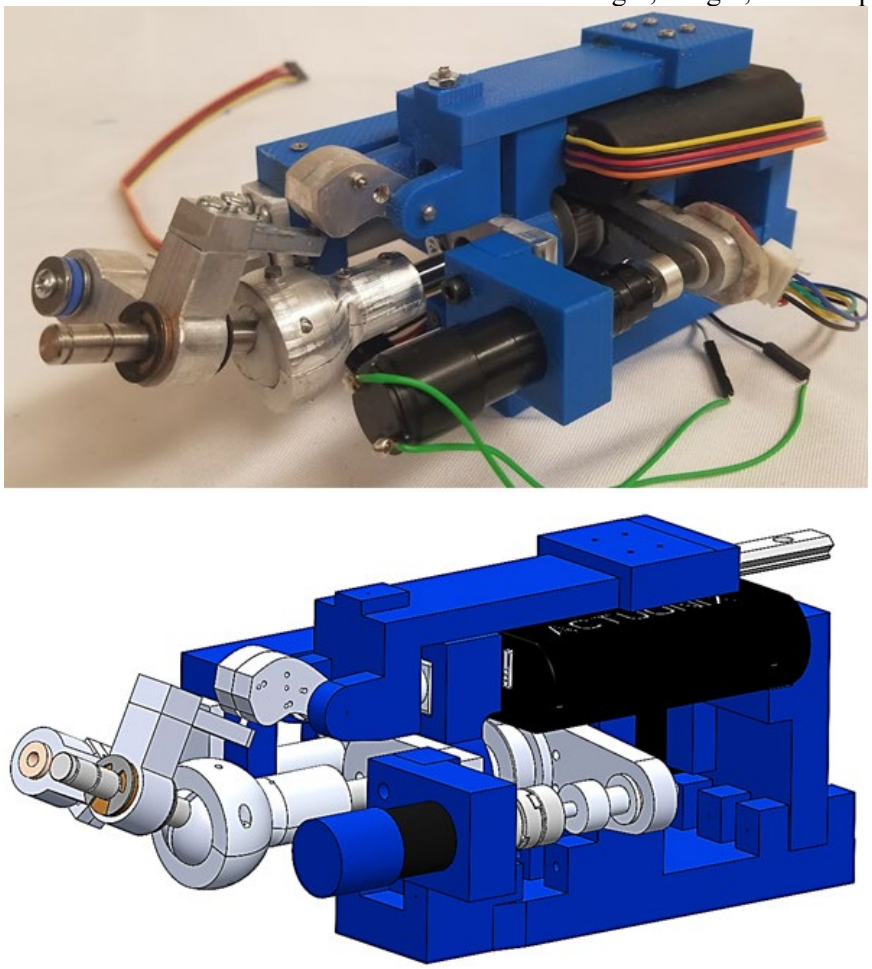

Figure 7. Prototype 3-DOF prosthetic wrist (top) and idealized CAD model (bottom).

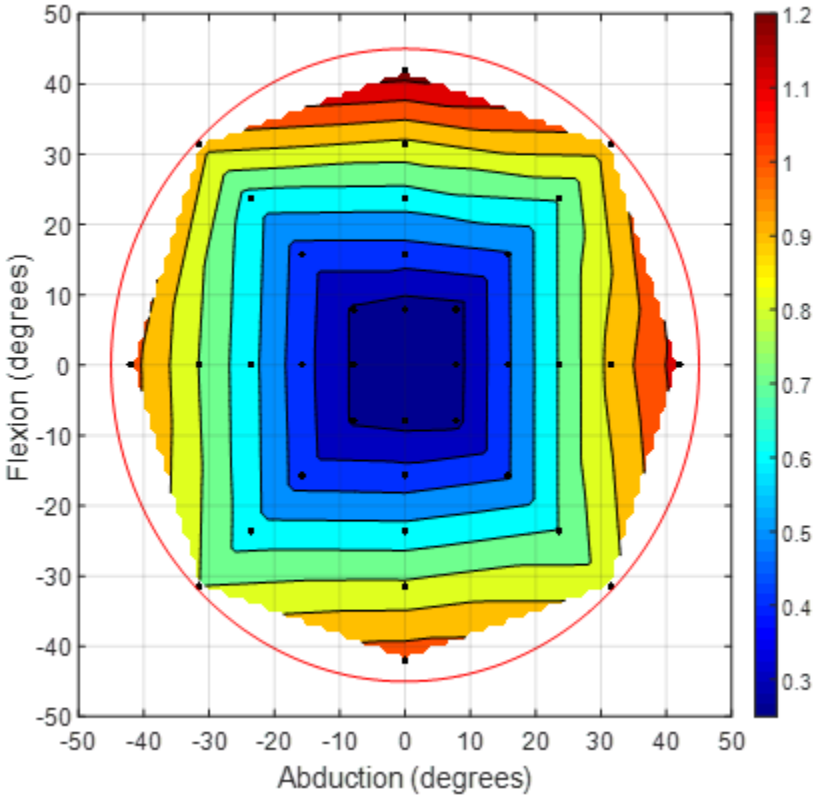

Figure 8. Time it takes (in seconds) to actuate from the neutral position (0,0) to the location in the workspace. The black points are the measured values, whereas the colored contour sections represent the interpolated values.

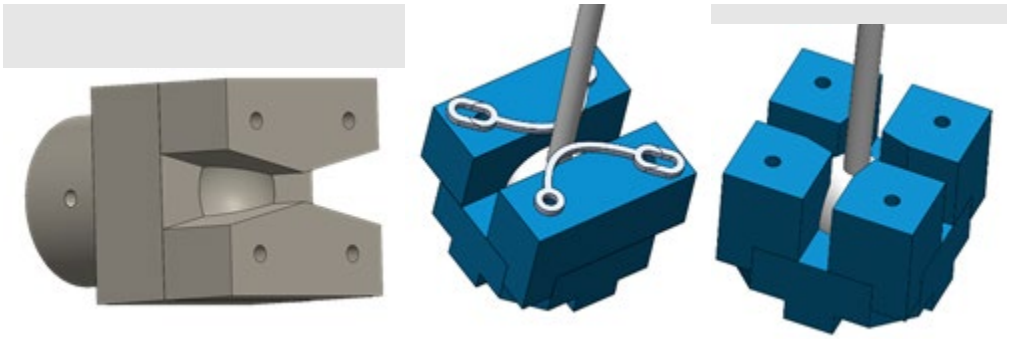

Figure 9. Different types of high range of motion spherical joints. (Left) static articular surface, stalls when stuck on central peak in channel. (Middle) Elastic articular surface, stalls when shaft presses against dead zone of white flexures but reconfigures as force on the flexure increases as flexure bends out of the way. (Right) 4 part static articular surface, stalls when touching interior corners but quickly snaps out of the way under increased contact force.

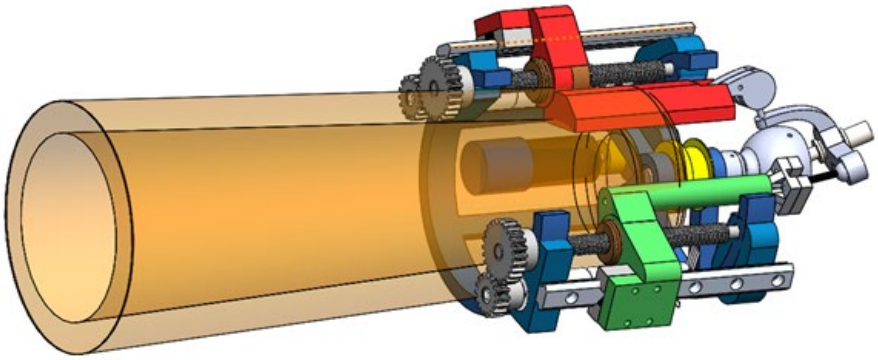

Figure 10. Surrounding socket wrist design. The overall additional length added to the end of the socket by the wrist is 2.25".

The group at Yale carried out initial design work for the prosthetic **hand device.** In particular, the following achievements have been made:

The final prototype of a single actuator myoelectric hand (Yale MyoAdapt Hand) was produced and evaluated in a preliminary benchmark and human subject test. In the benchmarking, sensor embedded objects were created to detect grip force. The hand was connected to a data logging software to measure average angular closing rate and closing rate of the fingers. Grasp aperture was measured mechanically using a digital micrometer measuring from the most distal aspect of the thumb and mating fingers in power and tripod or palm surface in lateral. Benchmarking and kinematic results are seen below.

TABLE I. BENCHMARKING RESULTS

Grasp Type	Grasp Specifications		Average Angular Closing Rates (°/s)			
	Grasp Force	*Closing Time*	*FF MCP*	*FF PIP*	*T MCP*	*T PIP*
Power	15.2 N	1.113 s	84.7	84.4	29.7	36.8
Tripod	3.6 N	0.476 s	145.0	99.8	39.9	136.5
Lateral	18.2 N	0.508 s	0 (fixed)	0 (fixed)	35.4	126.0

a. Only the index and middle finger are actuated in tripod grasp at twice the rate.

TABLE II. KINEMATIC CHARACTERISTICS

Grasp Type	Grasp Aperture	Range of Motion (°)			
		FF MCP	*FF PIP*	*T MCP*	*T PIP*
Power	113.8 mm	0-95	0-95	0-35	0-40
Tripod	113.8 mm	0-70	0-45	0-20	0-60
Lateral	25.4 mm	95-95	80-80	5-25	25-65

The Faulhaber brushed DC motor control board was used to sense current in torque control mode to determine when an object was grasped. When switching grasp types, slack in the system was either added or taken away using the DC actuator until a suitable pretension was achieved. In a six participant able bodied evaluation, participants scored favorably, moving an average of 19.1 blocks over a barrier in a minute in the Box and Blocks test and scoring an average of 82 IoF in the Southampton Hand Assessment Procedure (SHAP).

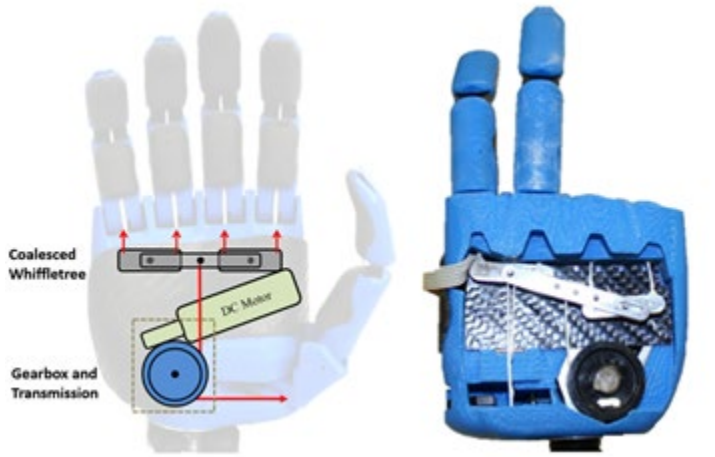

Figure 11. Final mechanism design for single actuator hand including the coalesced whiffletree differential, gearbox, pulley transmission and driving DC motor.

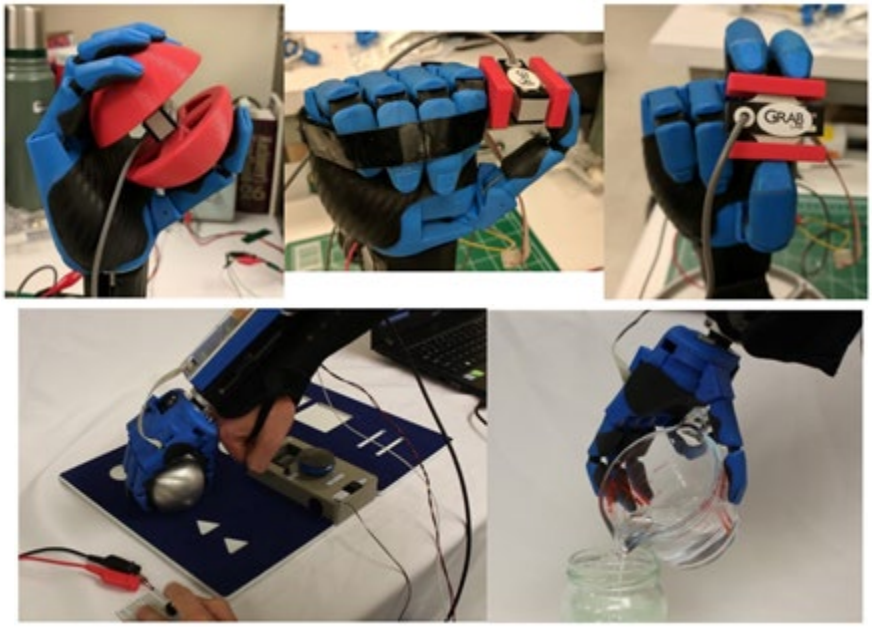

Figure 12. Benchmark testing in all three grasp types (power, tripod, and lateral) using sensor-embedded objects. Able-body testing was completed using a bypass socket that attached the prosthetic hand and electronics to the participants forearm. Able-body testing included completing five trials of the Box and Blocks test and a full Southampton Hand Assessment Procedure (SHAP).

Figure 13. Adaptive grasp from the underactuated fingers which are decoupled through the coalesced whiffletree differential. The power and tripod grasp have a large 113.8mm grasp aperture while the lateral grasp has a 25.4mm grasp aperture.

To develop a more effective single actuator prosthetic terminal device, a multi-stage optimization framework was developed to evaluate the stability of symmetric two finger underactuated grippers from a single actuator in open loop force control. This optimization included multiple stages, first anthropomorphic link lengths, palm

widths and pulley radius are sampled to determine configurations that provide stable contact for a range of object sizes. Next, stable configurations were evaluated to minimize post contact work commonly seen in underactuated grippers and to maximize the reliable stable object size. A weighted score was calculated based on these criteria and maximally performing configurations were tested for external disturbance resistance using the maximal resistible wrench criteria. A single configuration was experimentally tested to evaluate the accuracy of our model. Last, anthropomorphic design parameters of the maximally performing configurations were used to determine key parametric relationships for future design of stable robotic precision graspers that can stably contact a large variety of object sizes with minimized reconfiguration. External disturbance resistance is used to evaluate the stability of grasps post-contact with applications to path planning for robotic devices.

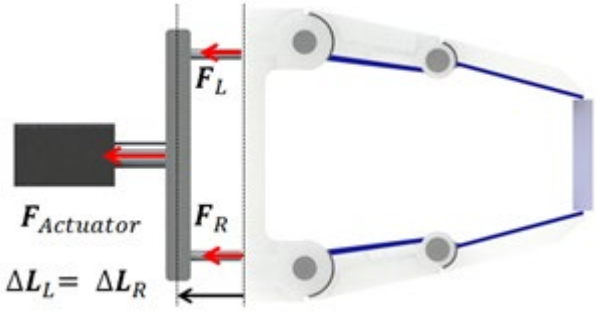

Figure 14. Model of a two-fingered underactuated tendon driven hand that is precision grasping an object in open loop force control.

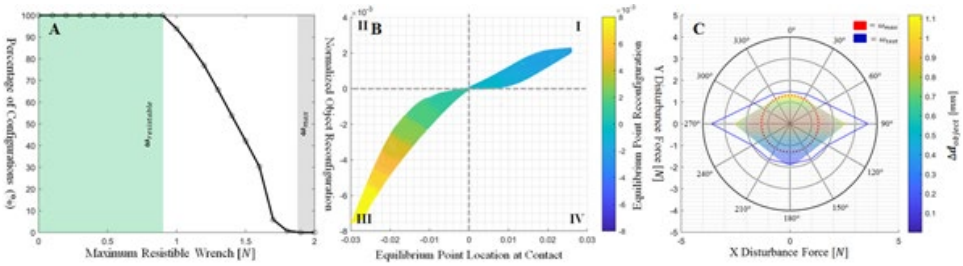

Figure 15. Three criteria used to evaluate the stability of the top 40% of maximum performing configurations. (A) Displays the percentage of configurations that can resists a certain maximum wrench in any direction, the green section shows the wrench at which all configurations could resist and grey section describes the cutoff for maximum resistible wrench. (B) Displays the equilibrium point reconfiguration relative to object reconfiguration to show that stable solutions reconfigure towards the contact force line of action, which acts as a force asymptote. In (C) simulated and experimental external disturbance plots are compared, the simulated resistible wrench is overlaid with object motion at the force and direction.

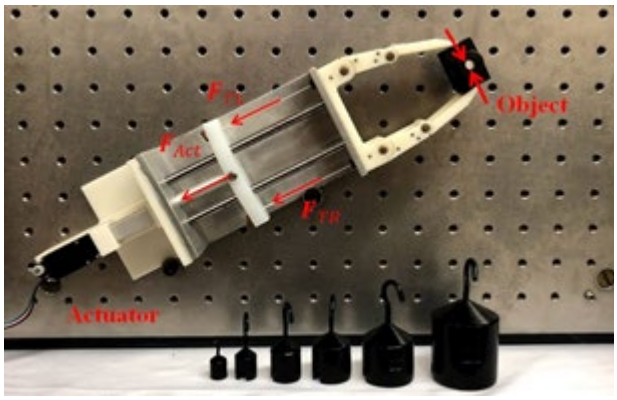

Figure 16. Experimental test setup including a linear actuator, coupled tendons, a hand and object. Weights were applied to the center of the object allowing gravity to apply a force in the global frame.

Year 4

The group at Yale carried out design and fabrication work for the prosthetic wrist device and explored ways to optimize the single DOF prosthetic hand. In particular, the following achievements have been made:

1. A 3DOF prototype that is wearable on either a bypass socket or prosthetic socket was designed and manufactured. Many of these components were designed to reduce to overall weight and size of the device while maintaining an acceptable degree of usability of the wrist device in terms of torque and speed requirements. This included motor selection and integration of drive-train and power transmission components into custom made structural elements.

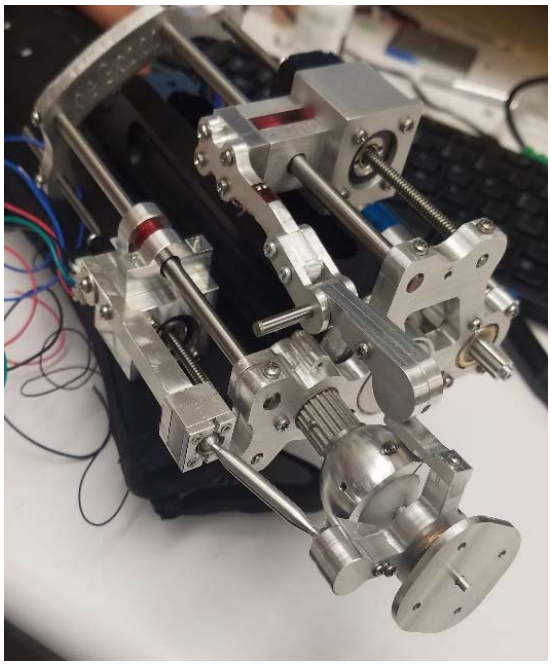

Figure 17. The new 3 DOF wrist prototype.

2. Multiple methods for providing feedback to the wrist device were explored. The feedback methods include indirect methods by measuring the motor positions and then solving the forward kinematics to determine the orientation of the wrist, and direct methods. The indirect methods implemented used magnetic contactless potentiometers to measure linear motor position with a low noise margin but significant additional hardware, and laser based solutions, which required little hardware but had significantly more noise. The direct method was implemented through use of state of the art inertial measurement units (IMUs), which capture the orientation of both the base of the wrist and the distal terminal device and can determine the wrist posture by calculating the relative orientation between the two.

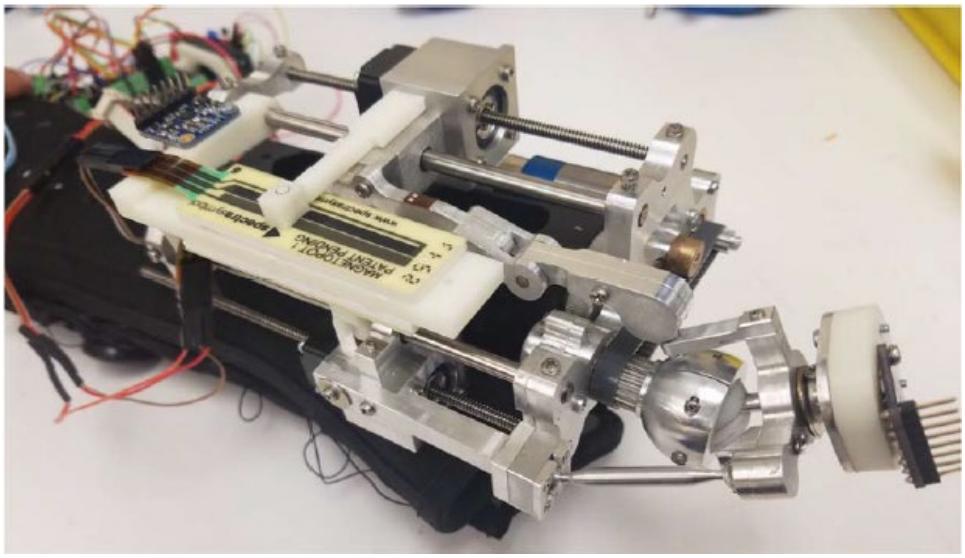

Figure 18. The new 3 DOF wrist prototype with the magnetic potentiometers and IMUs mounted on board.

3. Low-level control circuit boards were designed, manufactured, and developed to control the wrist. These boards handle the motor control and processing for the sensing elements. Two versions of these control boards were made. The first handled very basic motor control and required fast processing to control the wrist with high fidelity, and required multiple power supplies, thus many power cables and communication wires needed to go between the master device, controller boards, and the wrist. The second version handled power management, sensor conditioning, pulse generation for the stepper motors, and

over current protection fully onboard, reducing the amount of processing required for the master device. This increases speed and simplifies the control code.

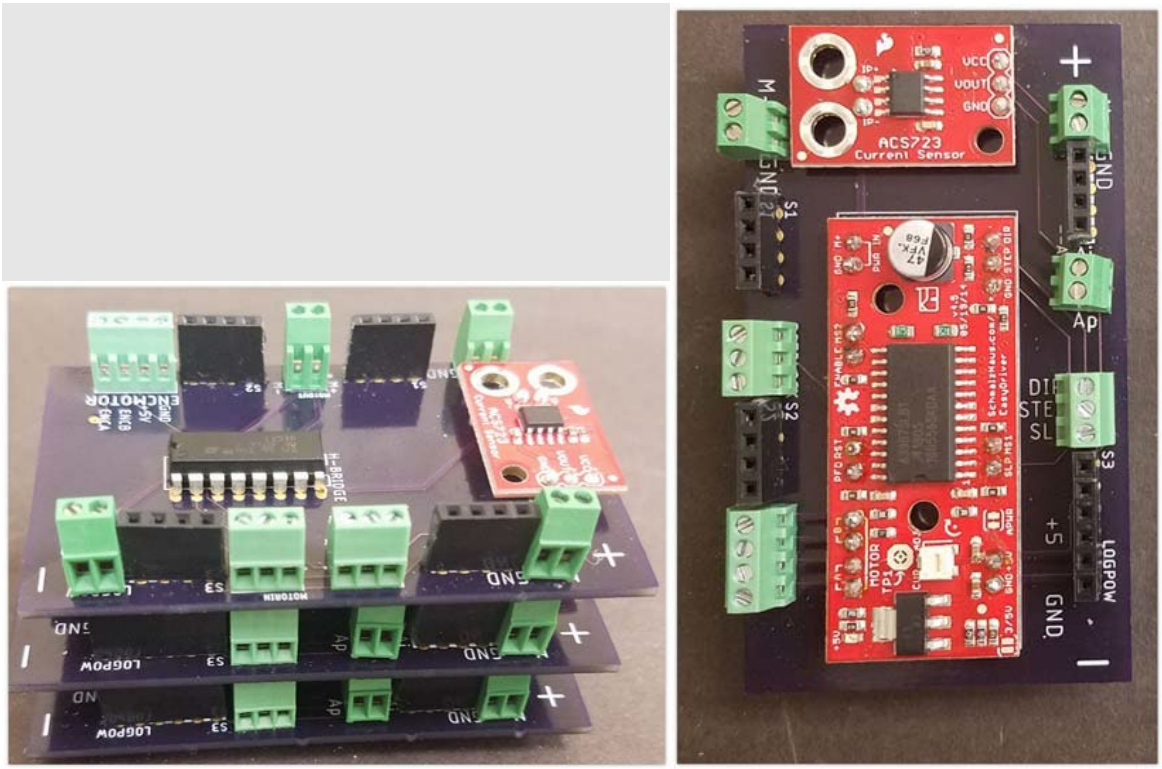

Figure 19. Version 1 of the wrist control boards. Stacked configuration on the left, exemplar individual board on the right.

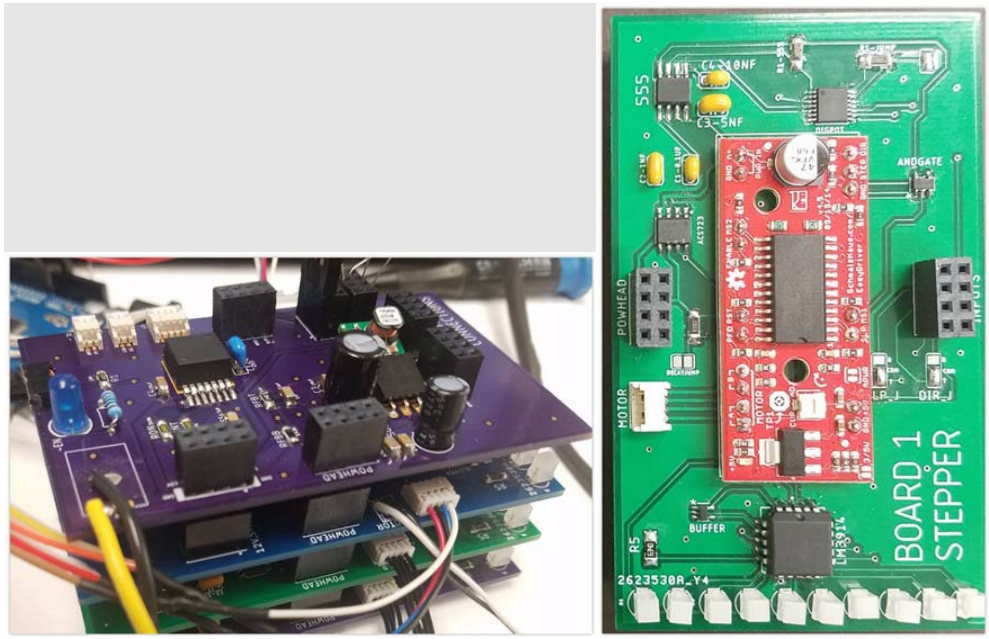

Figure 20. Version 2 of the wrist control boards. Stacked configuration on the left, exemplar individual board on the right. The boards were designed to stack to minimize horizontal footprint.

4. The finger parameters and gripping surfaces of a single actuator anthropomorphic prosthetic hand were optimized to be used in conjunction with the multiple degree of freedom wrist.
    a. A parameter search was completed to find optimal finger configurations for precision grasping from a single actuator. An optimization framework was created to evaluate the stability of the gripper for a variety of object sizes including heuristics on minimizing post contact work and maximizing the resistance to external disturbances while grasping. (Figure 21).

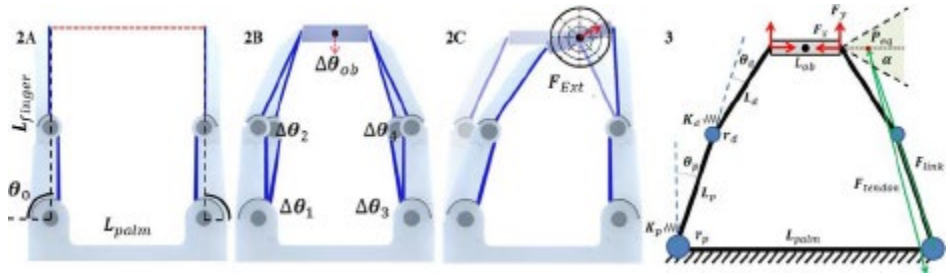

Figure 21. [2A-2C] The process for evaluating stability for two-fingered precision grasping including (a) the starting position of the hand and (b) a constrained optimization of the six bar mechanism to determine reconfiguration and (c) evaluating the stability of configurations to external wrenches. [3] A kinematic model of the two fingered system describing the starting positions, design parameters, kinematics and contact model.

b. The design of effective robotic finger pads was investigated for precision grippers or multi-fingered hands. The advantages and disadvantages of primitive geometries were compared to the performance of the human hand using a custom testing apparatus for rubber based gripping surfaces. (Figure 22).

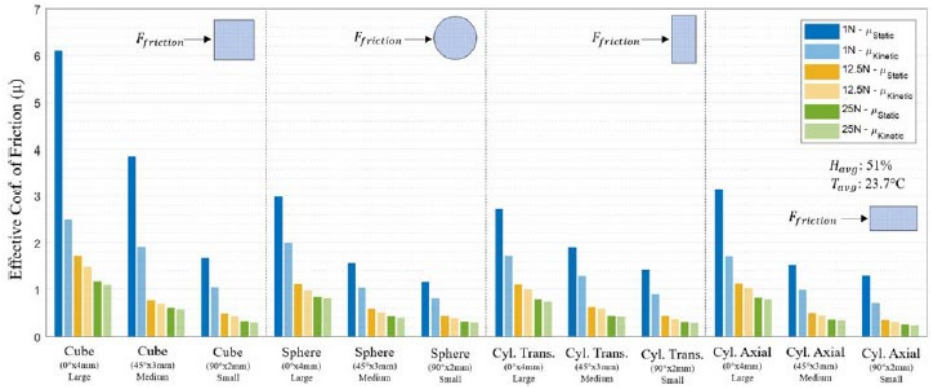

Figure 22. Evaluation of the variation in the effective static and kinetic coefficients of friction relative to a low (1N), medium (12.5N) and high (25N) normal loading force for the fabricated finger pad primitives. The three primitive geometries grip pads are listed in descending order from the pad of that geometry with the largest contact area and displacement to the smallest contact area and displacement. The cylinder is evaluated in two sliding modes, one sliding across the cylinder round or transverse direction and one sliding across the cylinder length or axial direction.

Year 5

The hardware development group at Yale carried out design, fabrication work for the prosthetic wrist device, and tested the wrist hardware, and explored ways to optimize the single DOF prosthetic hand. In particular, the following achievements have been made:

1. The prosthetic wrist device (Figure 23) was tested in a benchtop environment to characterize its performance as a wrist manipulator. Testing was done to characterize the mechanical performance of the device in terms of speed, torque, and backlash. The electronics and control algorithms were modified to optimize the performance of the wrist for use with human subjects.

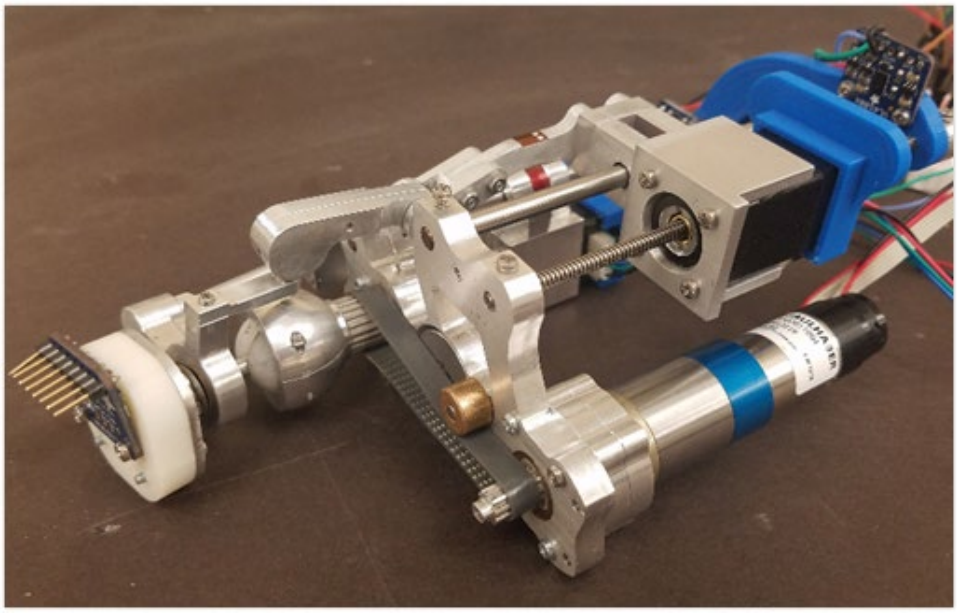

Figure 23. The 3 DOF wrist prototype.

2. Following bench top testing, a variety of sensing methods were tested on the wrist to return an estimate of its orientation. These estimates enable differing low level control modes of the wrist, from mirroring to gravity compensation to zeroing, for example. A sensor fusion algorithm was developed that utilizes many of the feedback strategies tested, and combines them to get a better estimate of the wrist position. A block diagram of the algorithm can be seen in Figure 24. This sensor fusion algorithm takes advantage of the non-backdrivability of the wrist device to determine its orientation and account for drift that would normally appear in inertial measurement unit (IMU) sensors. The three estimators are described in more detail below.

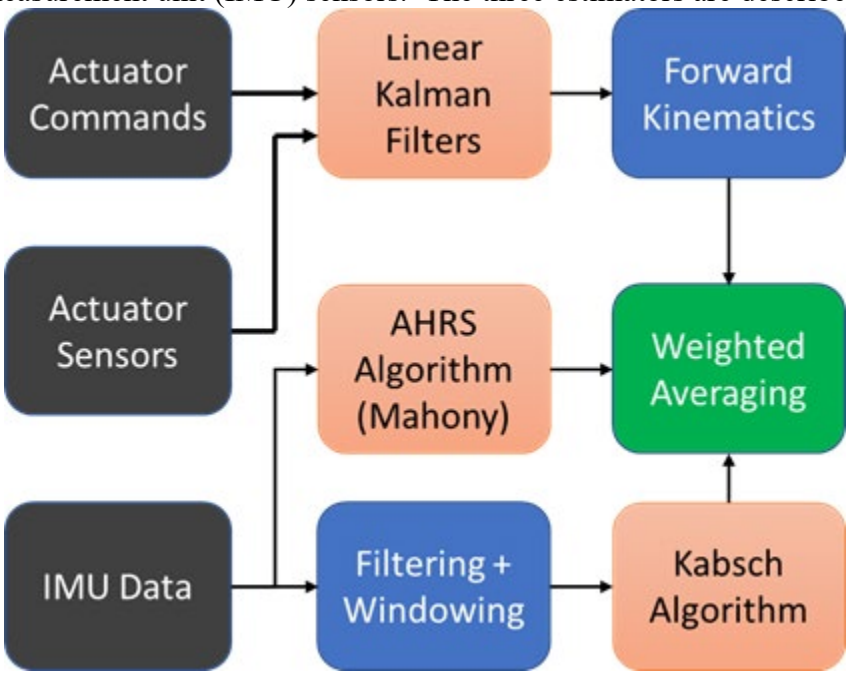

Figure 24. Diagram of orientation estimation algorithm. Black blocks correspond to data sensed from the wrist or known apriori, red blocks correspond to the individual estimators, blue corresponds to processing or selection steps, and green corresponds to the fusion algorithm, which outputs a weighted average of orientation based on the three estimates.

Estimator 1: A Linear Kalman Filter on joint sensor measurements used to estimate forward kinematics of the wrist. Because the geometric and kinematic parameters of the wrist are known, simple sensors (such as encoders and time of flight sensors), can be used to on the linear motors to determine joint angles. This can be implemented simply due to the decoupled nature of the wrist design, where each joint angle is largely only a function of one motor position. Each motor has its own Linear Kalman Filter to estimate its position, and these positions are then fed into the forward kinematics to estimate wrist angles. Figure 25. Shows an example of the estimated motor

position of the flexion motor via the filter, and how it corresponds linearly corresponds to the flexion angle estimated by Estimator 2.

Estimator 2: Relative rotation between two Attitude and Heading Reference Systems (AHRS). Both the base of the wrist and the hand have full 9 DOF IMU's mounted on them. Each IMU can feed data into a separate AHRS system, which then estimates the 3DOF orientation of each IMU. One may then compute the relative rotation between the hand IMU and the base IMU to determine the relative joint angles. Note that each IMU gives its position in a global reference frame, which can allow the software to know the hands orientation in a global frame as well. AHRS systems are sensitive to magnetic interference, but often result in steady and accurate measurements. However, they do take some amount of time and motion to initially converge, which can be seen in Figure 25. The predictions of two predominate AHRS algorithms are shown in Figure 26.

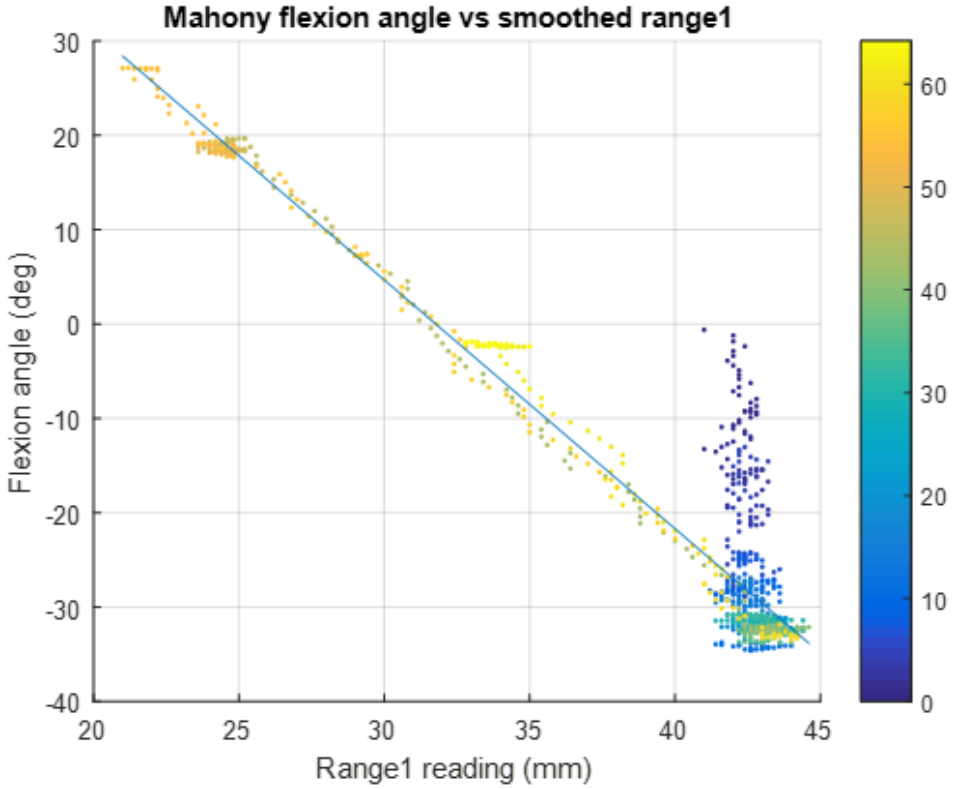

Figure 25. Plot of estimated flexion motor position from Linear Kalman Filter and AHRS estimated flexion angle, with color corresponding to the time the sample was taken (in seconds). The large strip of blue points corresponds to early in the trial, when the AHRS estimator (Estimator 2) was just turned on and had not yet converged to the true flexion angle, though the range readings passed through Estimator 1 were already quite near the proper value of 42mm. Note that the blue points correspond to time <15 seconds, when the AHRS was still converging. Post convergence, the estimated motor position quite linearly tracks the estimated flexion angle.

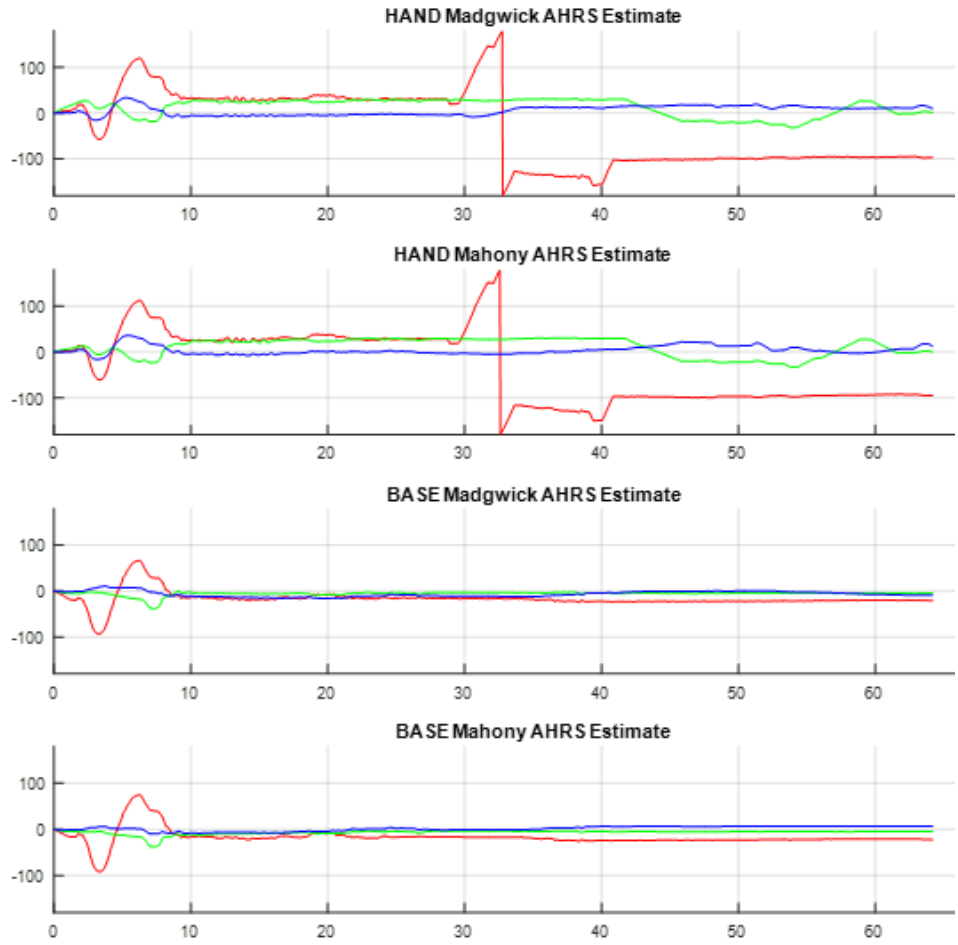

Figure 26. AHRS estimates of hand and wrist base orientations in global coordinate frame. From top to bottom, Madgwick AHRS estimate of the hand orientation, Mahony AHRS estimate of the hand orientation, Madgwick AHRS estimate of the wrist base orientation, and Mahony AHRS estimate of the wrist base orientation. Blue = pitch, green = yaw, red = roll. Note that when the ame type of motion appears in base and hand graphs, it corresponds to the entire wrist and hand moving as a rigid body. However, when there is only motion in the top graphs, this corresponds to the wrist itself actuating.

Estimator 3: Kabsch algorithm relative orientation estimate. The Kabsch Algorithm in general is a method for calculating the optimal rotation matrix between two paired sets of points. While the two sets of points are usually positions, or points on an object, before and after rotation, in this case, we use both accelerometer and gyroscope measurements from the base and hand. When the wrist is not actuating (i.e. when the orientation of the hand is not moving in relation to the base of the wrist), but the overall hand-wrist system is experiencing motion (say, by moving the shoulder and elbow while the wrist is locked), the accelerometer/gyroscope data from and hand and base are simply rotated versions of one another. Example accelerometer data is shown in Figure 27.

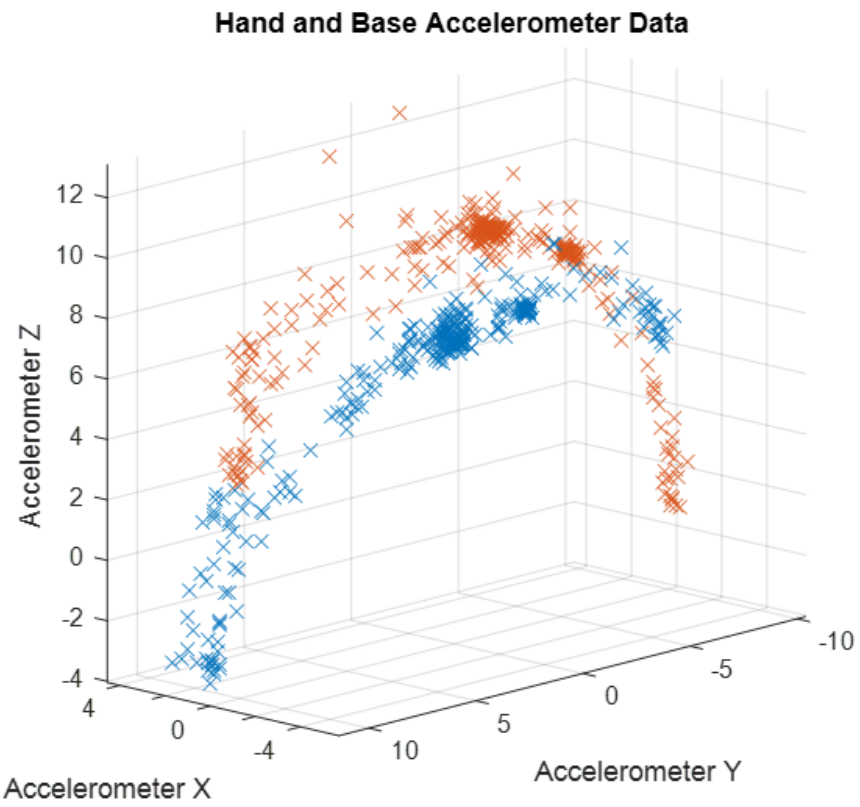

Figure 27. Scatter of accelerometer data from the hand IMU (blue) and the wrist base IMU (red). Both sets appear to be semicircular arcs in 3D space, both with similar features (e.g. the clusters near the top of the arcs). These clusters correspond to one another, and a rotation that maps the blue set onto the red set can be easily found using the Kabsch algorithm.

To evaluate the usefulness of this the Kabsch estimator, we simulated wrist and hand motion with measurement noise, a varying number of paired point observations, and how these two components affect the error of the algorithm. The results of this simulation can be seen in Figure 28.

To simulate this, we created one set of points which corresponded to the base of the wrist accelerometer/gyroscope measurements. To generate the second set of points corresponding to the hand accelerometer/gyroscope measurement, we applied a constant rotation $\boldsymbol{R}$ to the first set of points, but injected noise after the transformation. Injecting noise simulates either a noisy sensor reading or the sensor not being mounted rigidly. The amount of noise was varied to determine how high the signal to noise ratio (SNR) needed to be to remain under a certain amount of error in estimating $\boldsymbol{R}$. We then further considered changing the number of paired data points to be fed into the Kabsch algorithm to see if error changed with the number of observations. We found that with a modest SNR of 0 (if the measurement noise was nearly as large as the signal itself), with a high enough number of obersevations, one could still estimate $\boldsymbol{R}$ to within 20°. In practice, the SNR is much higher than 0, and it only takes approximately 20 observations to achieve <5° error in estimating $\boldsymbol{R}$.

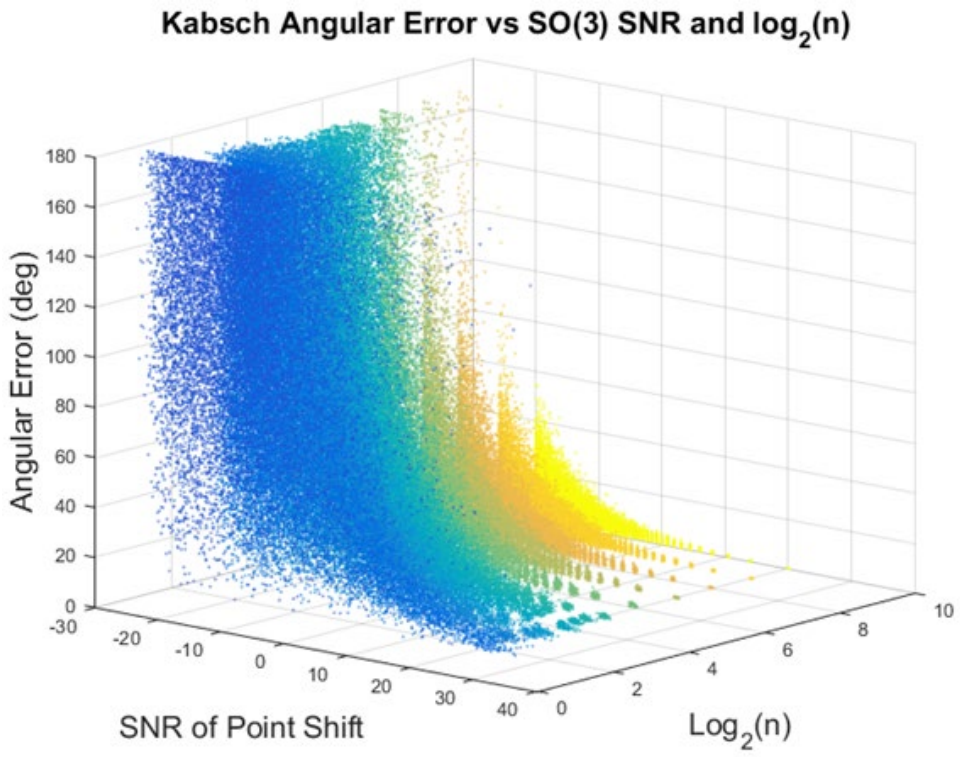

Figure 28. Error of the Kabsch algorithm in estimating ***R,*** measured in degrees from the actual rotation, as a function of the SNR of the measurements and the number of measurements taken (log scale). The colors correspond to different number of measurements taken, ranging from only two measurements taken (dark blue) to 1024 measurements(yellow). Note that eve with 16 measurements taken (green), and a modest SNR of 10, the estimate is quite accurate. Also note that the maximum error one can have is an error of 180°, which would correspond to estimating the completely opposite rotation.

To combine these estimates, we also developed a scheme to take into account the estimates' errors (which themselves also estimated) in a weighted averaging scheme (green box in Figure 24). The higher the estimated error, the less weight that one of the estimators would receive in the averaging. We use a common quaternion averaging scheme that minimizes the geodesic distance between the three quaternions.

Methods to generate input for the prosthetic device were tested. Angle estimation of the healthy unaffected arm was carried out outside of the motion capture environment to determine suitability of using IMUs on the healthy arm as a means of controlling the prosthetic wrist. One IMU is mounted on an elbow brace to track the orientation of the forearm in space, and another is mounted to the subject's hand to track the hand's orientation in space. The wrist orientation of their healthy arm can be deduced by the relative orientation between the forearm and hand, and this orientation can then be mirrored on the prosthetic wrist on the contralateral side. Setup and estimates may be seen in Figure 29. This system was validated using fiducial markers and an optical camera system.

Figure 29. Opposite arm fitted with an elbow brace and IMUs (one distal to elbow and one mounted on hand). The elbow brace is used to provide a mounting point for the IMU to decouple the upper arm motion from wrist motion. This allows the system to determine the wrist angles through the relative transformation from the elbow IMU to the IMU on the hand. Without the elbow brace, skin stretch while pronating and supinating would greatly affect the angle measurement.

3. Development of a high range of motion spherical joint (Figure 30) that allows a much greater range of motion than commercial off the shelf joints. This work was presented and published at ASME IDETC 2020. The spherical joint can be used in a variety of parallel mechanisms and implemented at a variety of size scales.

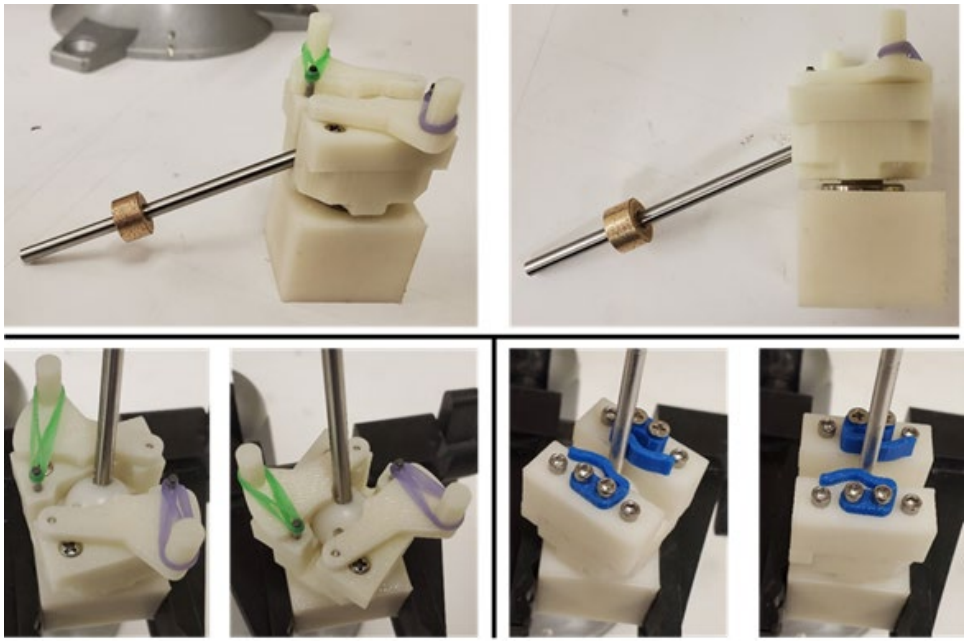

Figure 30. High range of motion spherical joint prototype. The top row of images shows the large displacement from the center of the workspace of the joint (i.e. a vertical orientation). The lower left images show one prototype which uses elastic bands and rigid elements to act as springs, which allows the joint to reconfigure into the large range of motion direction when the output shaft makes contact. The lower right images show a prototype which uses flexible elements to achieve reconfiguration.

4. The researchers conducted a preliminary test of the usability of the prosthetic wrist while manipulating a few exemplar objects. The testing served to highlight which parts of the system needed to be improved before human subject testing. Most notably, the input to output lag needed to be addressed. This lag was reduced by offloading more processing from the local microcontroller to the PC. An example manipulation may be seen in Figure 31.

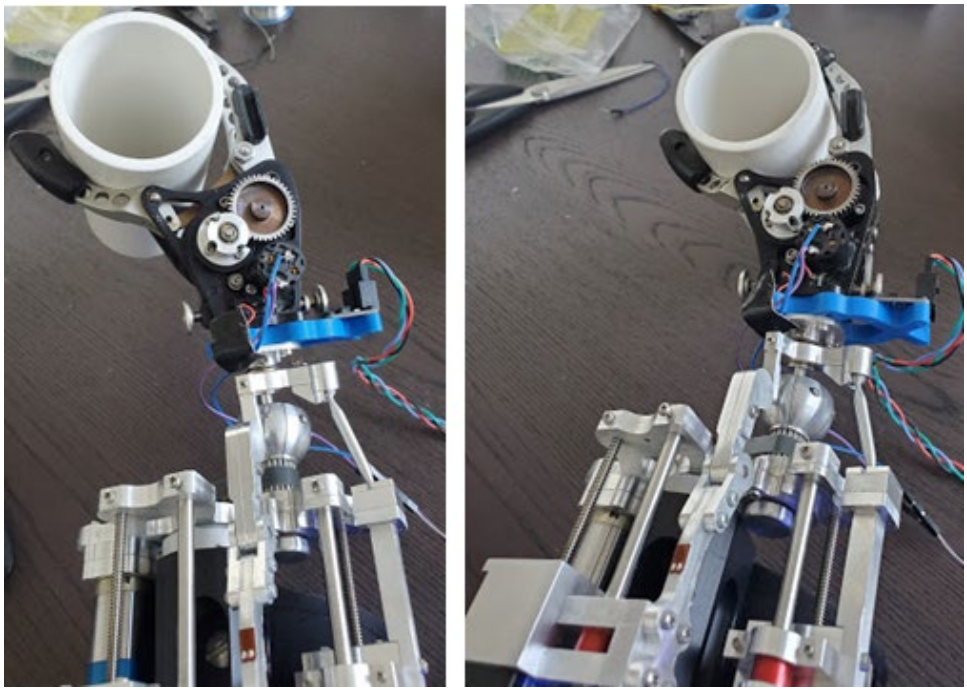

Figure 31. Exemplar object #1 (cylinder) manipulated by prosthetic wrist and 1DOF Hand.

5. The finger parameters and gripping surfaces of a single actuator anthropomorphic prosthetic hand were optimized to be used in conjunction with the multiple degree of freedom wrist. The finger parameters were then translated to a physical single actuator prosthetic hand that was fabricated.

a. A parameter search was completed to find optimal finger configurations for precision grasping from a single actuator. An optimization framework was created to evaluate the stability of the gripper for a variety of object sizes including heuristics on minimizing post contact work and maximizing the resistance to external disturbances while grasping. The optimal designs for precision grasping were tested – both in simulation and experimentally - to evaluate stability both during grasp acquisition and resisting external disturbances (Figure 32).
b. A full single actuator robotic hand with three grasp types was designed with input from all previous optimization and design studies. This had will be tested both through benchtop testing and with able bodied / amputee participants in the near future (Figure 33).

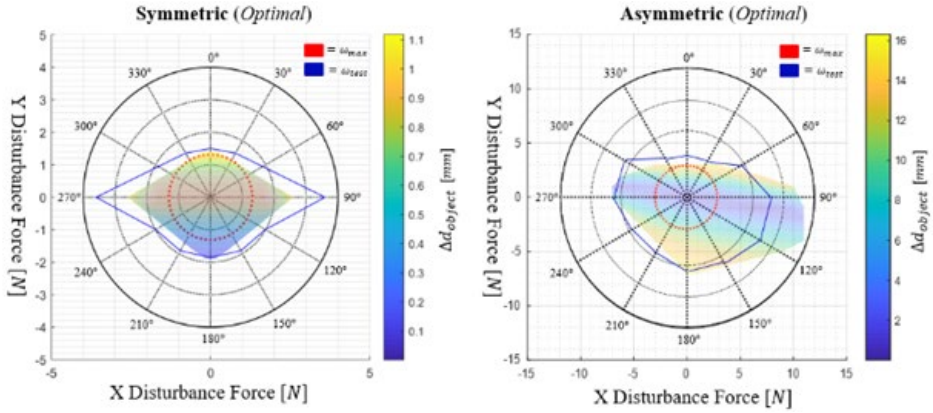

Figure 32. Two heuristically optimal configurations, one symmetric and one asymmetric, were fabricated and experimentally evaluated under externally applied disturbances after reaching full actuator load. The left shows the symmetric resistance until failure and the right shows the asymmetric resistance until failure – both in 30 degree increments representing the twelve evaluated loading directions.

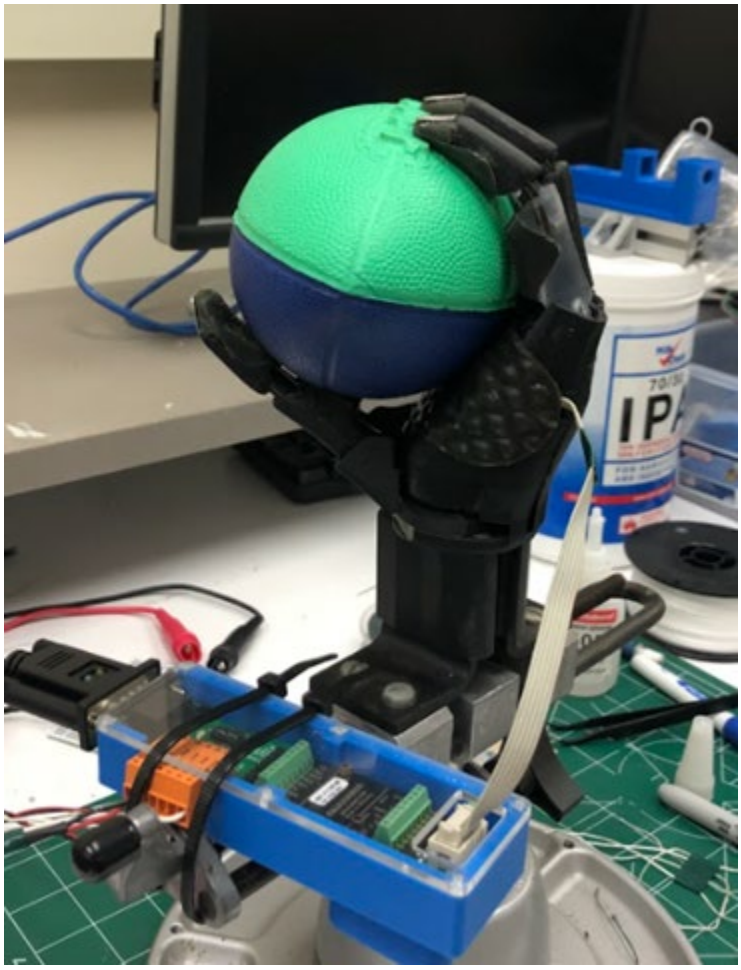

Figure 33. Optimized single actuator prosthetic hand reconfiguring around a soft object in "wrap" grasp.

Yale Software & Control Group Accomplishments

The Software and Control group at Yale worked on developing a virtual reality environment in which testing different control strategies on simulated prosthetic arms would be possible. The prosthetic arms spanned various joints, with varying degrees of freedom. Moreover, this system was incorporated into a motion capture environment to allow the researchers to quantify movement on test subjects using different simulated arms and control strategies.

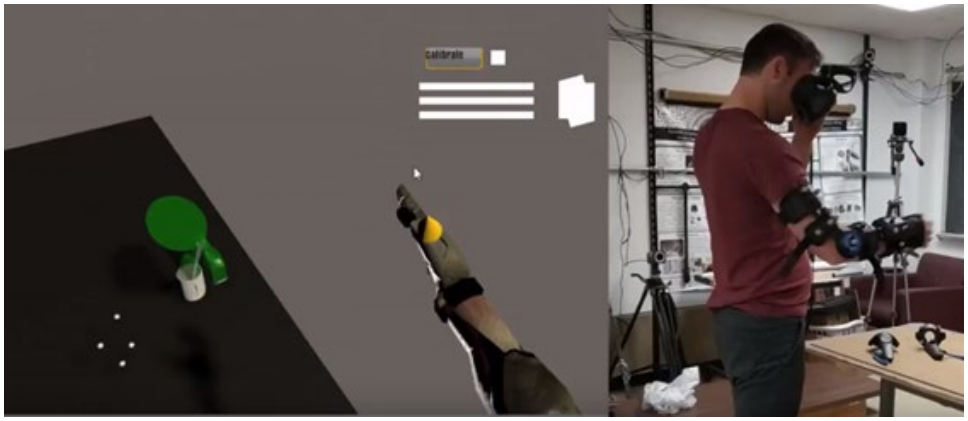

Figure 34. A researcher demonstrating how the reflective markers (right) on the real arm are used to place a simulated prosthesis into the virtual environment (left). The virtual prosthesis will perform simulated tasks, such as drinking out of a cup (left). The virtual environment (left) is displayed in the goggles (right). Additionally, an elbow brace can be seen worn by the researcher which constrains the wrist movement necessitating the operation of the prosthetic wrist device.

1. We developed a virtual reality platform to supplement prosthesis adapters. This included purchasing and setting up the VR equipment (HTC Vive), developing a virtual environment in Unity, creating controller

commands to operate the prosthesis, and using the motion capture set up (Vicon) to streams a user's arm position into the environment. An example of the virtual environment can be seen in Figure 34.

2. A variety of input methods were designed to allow a user to control the virtual prosthesis using differing control strategies. These ranged from traditional sequential control of prosthetic devices utilizing EMG as a means of communication between the subject and the system, simultaneous control using a controller with 7 buttons held in the opposite hand for multi DOF control, and a simple joystick to provide an intuitive interface for each wrist control mode in Virtual Reality.
3. The virtual environment was designed and optimized to allow for subjects to complete virtual tasks, including manipulating objects. For this, grasping functionality was added into the virtual reality environment, manipulatable objects were created, and task completion criteria we developed and incorporated as well. Several improvements were made to the virtual reality testing platform by implementing better visual cues, interface changes, and implementing more responsive control.
4. A Vicon motion capture system was integrated into the virtual reality system to allow streaming the subject's limb and body position into the virtual environment, as well as to measure the subject's motion profiles as they perform tasks in the virtual environment. The motion capture environment was refined to allow for capturing motion of the torso and the pelvis, which can thus be used to infer compensatory motion due to the lack of some degrees of freedom in the simulated prosthesis.
5. An experiment was conducted to evaluate both the virtual environment and the control methods subjects could use to complete tasks in the virtual environment. The experiment required that we collect motion data coming from all sides of the human body. We re-aimed and re-focused the cameras such that we captured the data with maximum fidelity.
    a. As part of the experiment design, we implemented 5 different wrist control modes: healthy, fully constrained wrist, sequential control, simultaneous control, and trajectory control. Experiment was designed to analyze whether users had a control mode preference, how long training took, and how long it took users to complete the tasks.
    b. Subjects used a joystick (HTC) input to simulate both a two-site EMG control (standard input in real myoelectric devices) and a theoretical input where users have simultaneous access to all degrees of freedom. See Figure 35 for set up. Results, including time to complete, can be seen in Figure 36.
    c. A limited version of the study was performed by a subject using EMG (Figure 37), to confirm that the virtual reality set up closely mimics the real world as well as to verify results previously obtained when using the joystick. Two EMG's were placed on opposite sides of the forearm and should mimic the placement of real EMG's of a myoelectric wrist. Muscle activation was tracked using an Arduino Uno and stream to Unity. Preliminary results are displayed in Figure 38.

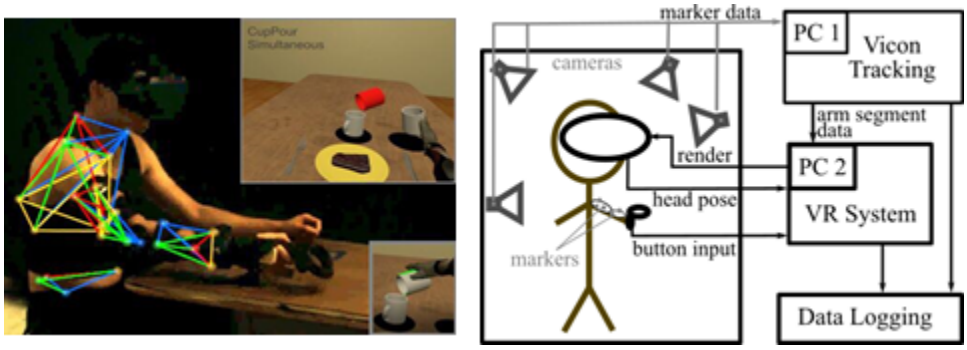

Figure 35. (a) The virtual reality experiment set up consists of live motion tracking (left), joystick input (left), and displaying the inputs to the head mounted display (top and bottom right). The tasks consisted of orientating and placing the end effector in desired places indicated in red (top right) and satisfied by changing the color to green (bottom right). (b) Flowchart depicting the data processing.

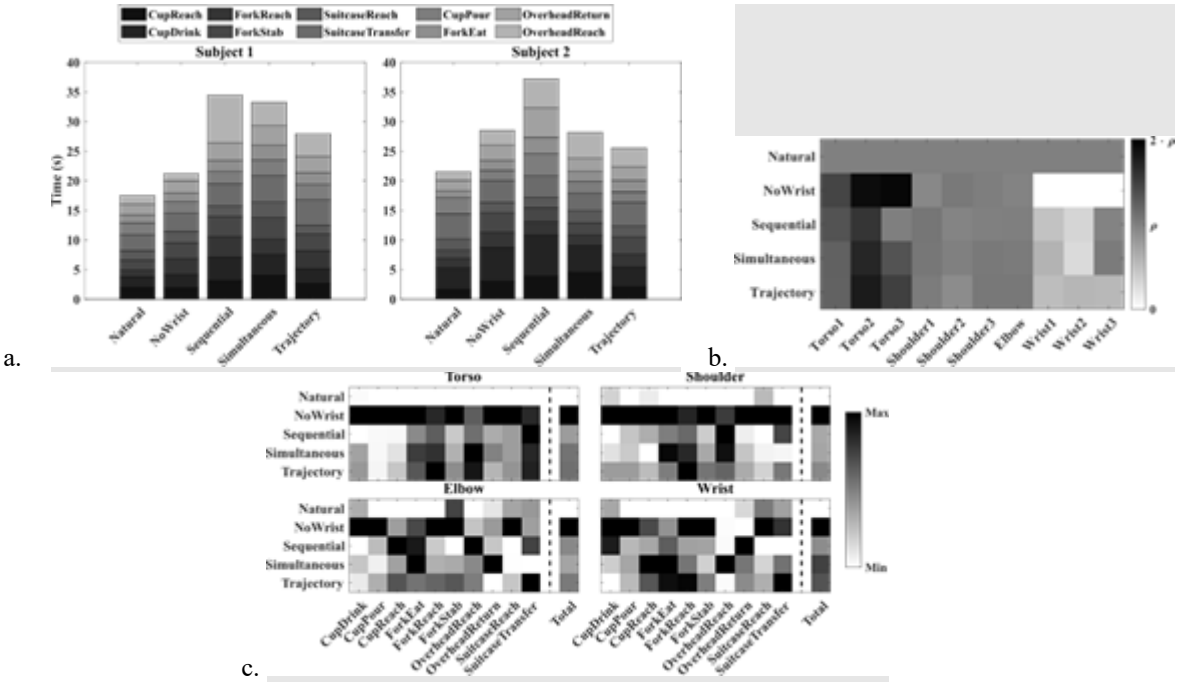

Figure 36. (a) Time it took each subject to complete the experiment protocol using each of the 5 wrist control modes. (b) Average range of motion of the wrist, forearm, shoulder, and torso joints exhibited during the experiment. (c) Cartesian trajectory length is displayed for the torso, shoulder, elbow, and wrist, during each of the tasks.

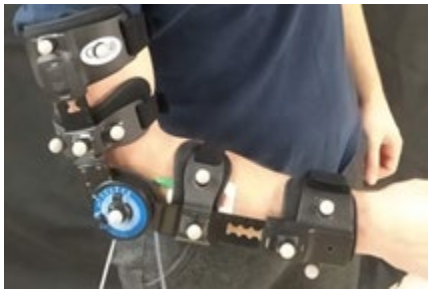

Figure 37. Motion tracking markers are placed around a brace to provide a consistent marker layout across subjects. The range of motion was not limited in brace. Below the brace, 2 EMG's can be seen, which track the user's flexor and extensor muscle groups.

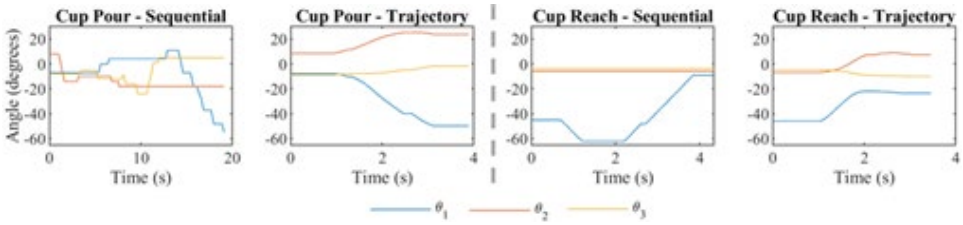

Figure 38. Results from a single subject comparing the proposed trajectory control to the sequential control methods for a virtual prosthetic wrist using EMG input. The angles correspond to supination, flexion, and ulnar deviation, in that order.

Following the preliminary testing of the virtual reality protocol testing outlined above, we made further progress testing a virtual reality control environment for our device designs, as outlined below:

1. All 12 subjects have completed the Virtual Reality protocol testing the novel trajectory controls for three different prosthetic devices
2. Subject data was processed and analyzed, which includes the qualitative surveys and the quantitative subject measurements for the Virtual Reality protocol.
3. A final single actuator prosthetic hand with multiple grasp types was fabricated including optimal kinematic parameters from previous studies.
4. A control interface for the 3DOF wrist was completed and is now ready for final testing.
5. Qualitative survey results (Figure 39) have been processed suggesting that that there are certain benefits of trajectory control that are worth exploring further. Additionally, quantitative subject measurements

include time to complete the experiment with each of the test conditions (Figure 40), Cartesian path travelled by each of the body segments (Figure 41), and range of motion of each joint angle (Figure 42).

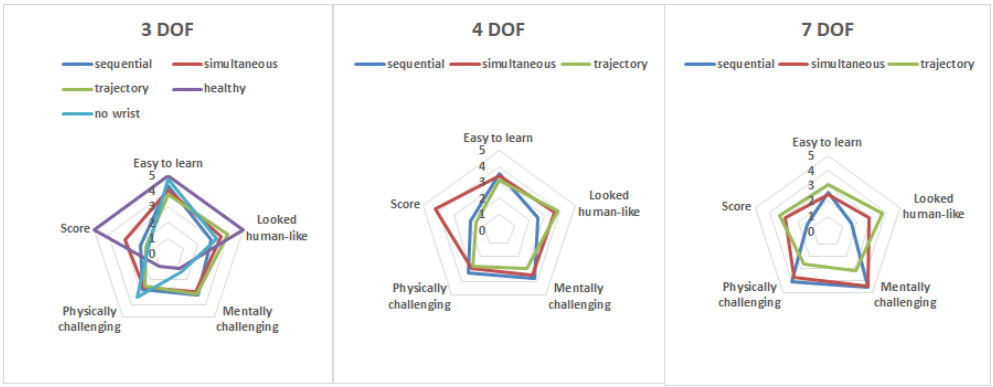

Figure 39. Survey results assessing subject opinions of the three different prosthetic devices (3, 4, and 7 DOF) with the different control methods (sequential, simultaneous trajectory, etc.).

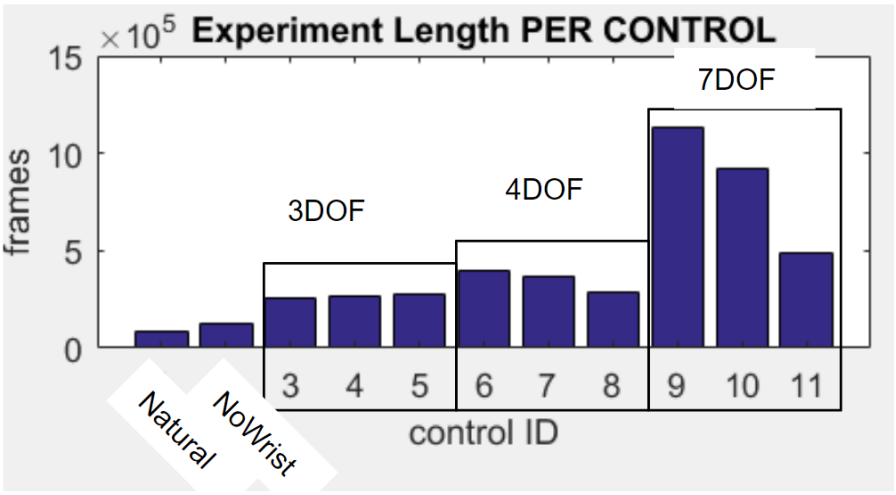

Figure 40. Time (measured as number of frames) for each of the testing conditions.

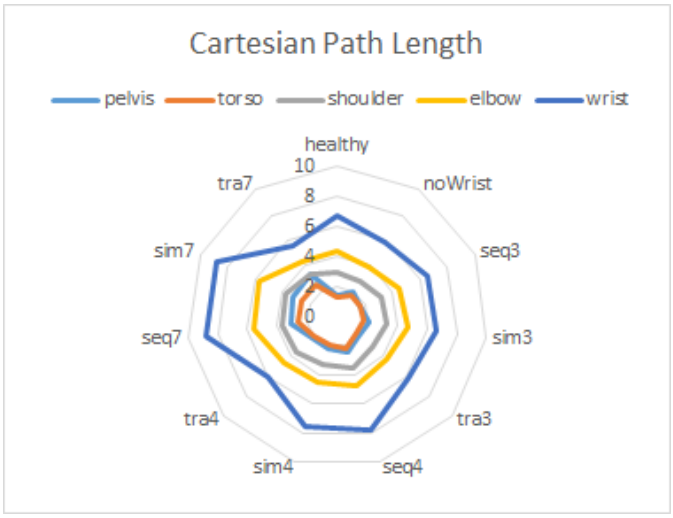

Figure 41. Path length travelled by each of the body segments.

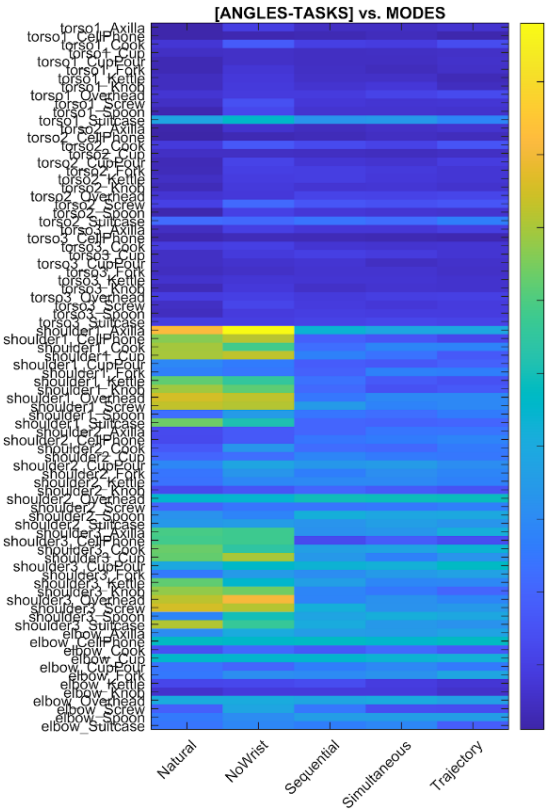

Figure 42. Range of motion results for each of the joint angles displayed as a heatmap.

.

1. Using the kinematic parameters and finger pad surface geometries optimized in previous studies a multi-grasp multi-DOF prosthetic hand and associated testing hardware were fabricated (Figure 43) to be evaluated in a human subject testing trial.

Figure 43. Final single actuator prosthetic hand with three grasp types. The hand is fabricated from 40% glass infill ABS composite, urethane gripping surfaces, aluminum core components and stainless steel fingernails.

2. Joint angles were verified using IMUs. The IMUs or the motion capture system can now be used to determine the user's intent on where they would like the wrist to move by mirroring the desired action on the healthy arm.

3. A climbing control strategy (Figure 44) was implemented to control the prosthetic wrist hardware. This was necessary because the position of each of the actuators limits the full range of the opposite actuator (Figure 45), due to the fact the wrist workspace is circular.

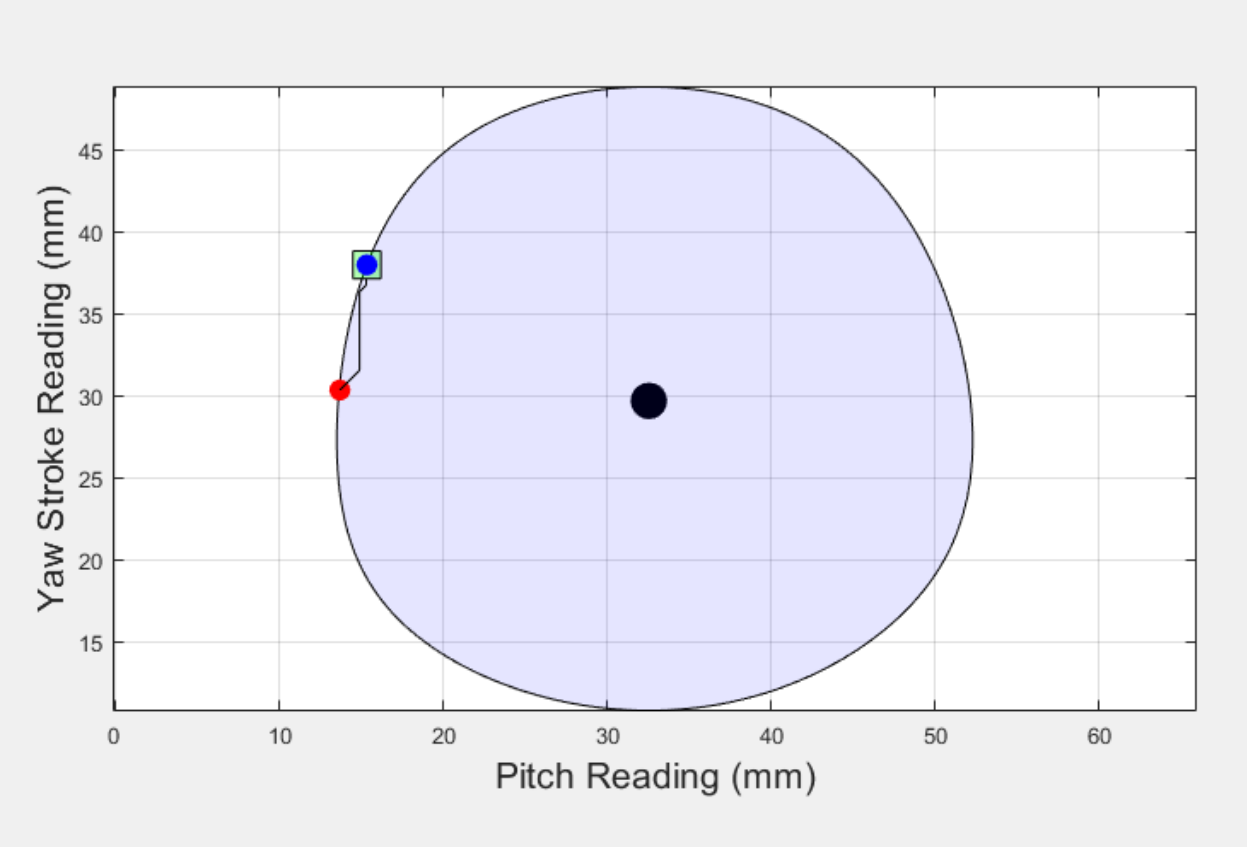

Figure 44. Climbing controller. As the wrist attempts to move from the blue position to the red position, if both actuators were moved at full speed, the output shaft of the wrist would collide with the workspace boundary, causing potential damage. To simplify the control, instead of varying the speed of the actuators, turning the offending actuator off when it would cause contact results in a climbing motion on the edge of the workspace.

4. Wrist hardware was redesigned to allow for greater social distancing and sterilizability. High touch components are now replaceable – either 3d printed or low cost, off the shelf components.

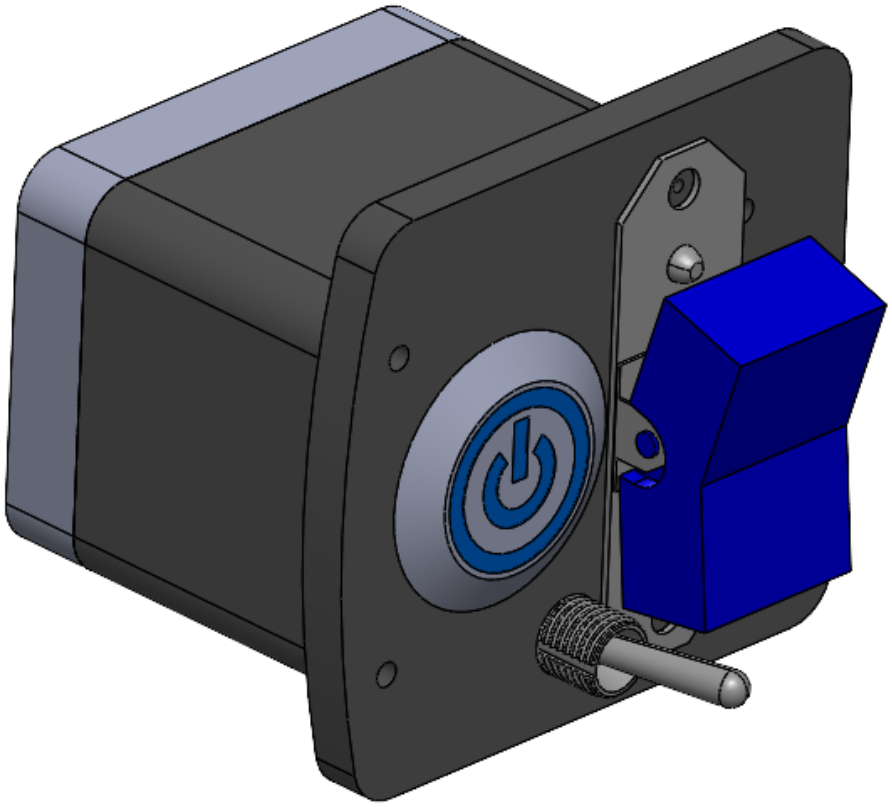

Figure 45. Opposite hand controller for prosthetic wrist human subjects testing. Excluding the electronics, the controller can be 3D printed, resized for different subjects, sterilized and replaced. The purpose of the controller is for the user to be able to communicate their intent for the wrist to move, return to neutral position, and open and close the hand by interacting with the button and switches.

5. A visualizer (Figure 46) was designed to help human subjects visualize wrist position. A visualizer in 3D as well as a 2D projection were tested for both speed, clarity, and understandability. While the 3D visualizer yields more realistic information, the 2D visualizer was found easier to understand.

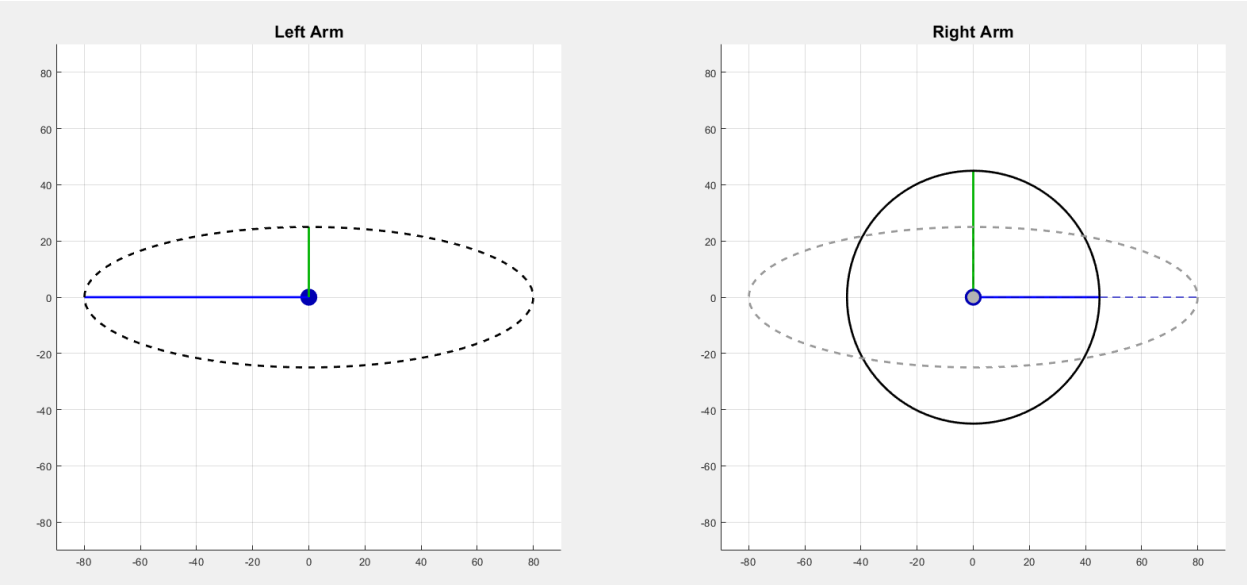

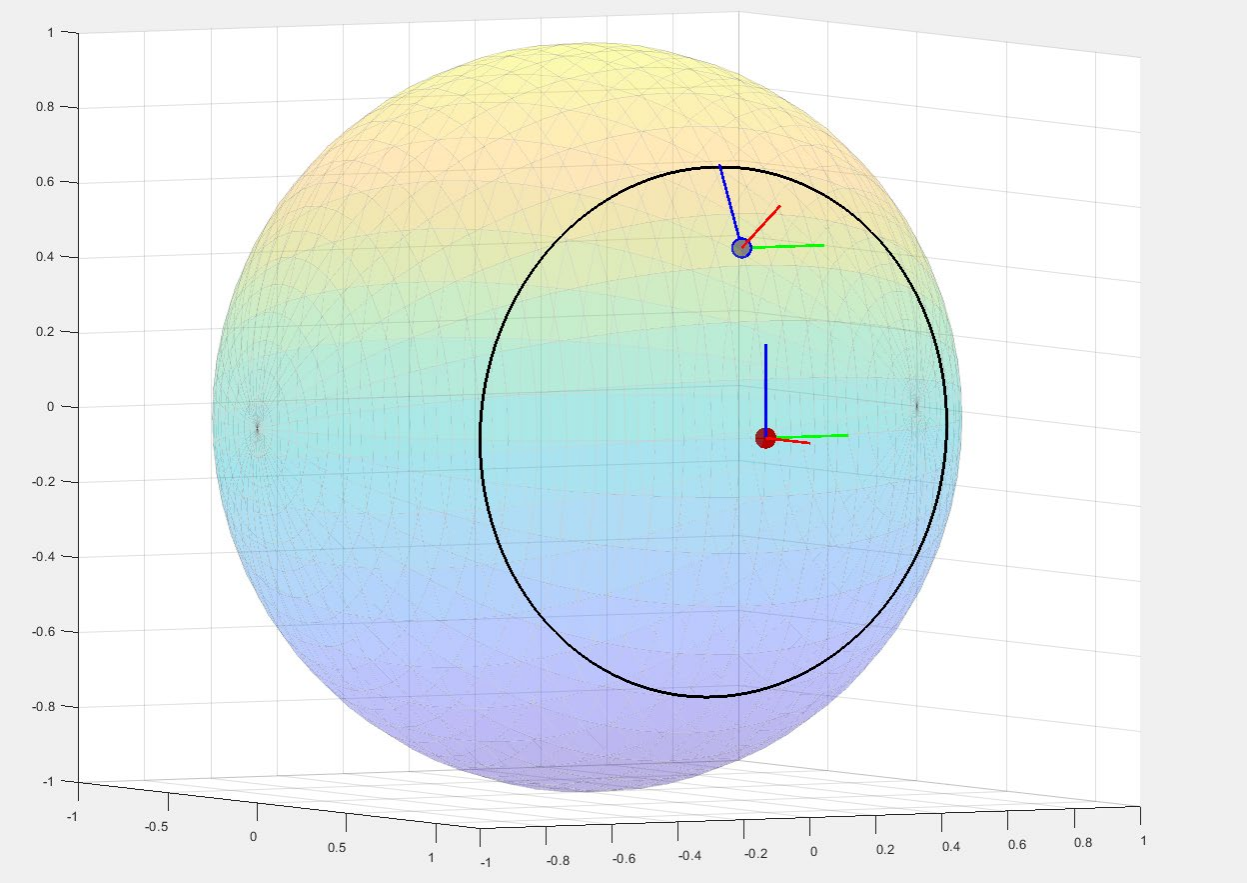

Figure 46. 2D (top) and 3D (bottom) visualizers. These visualizers would assist a subject in moving the wrist to the desired orientation by informing them where the wrist currently is in orientation space, and where their target currently is. When the wrist is at the target position, the "frames" (i.e., the sets of lines in each picture), would be aligned.

NCSU Group Accomplishments

Year 1

The group at NCSU focused on myoelectric control and established the block diagrams of two different decoding algorithms. Particularly, the following achievements have been done:

1. Different EMG decoding algorithms have been explored to control the 3-DOF of wrist.
2. Block diagram of the control scheme for EMG-Driven musculoskeletal model (Figure 47) has been designed.
3. Block diagram of the control scheme for Kalman filter (Figure 48) model has been designed.

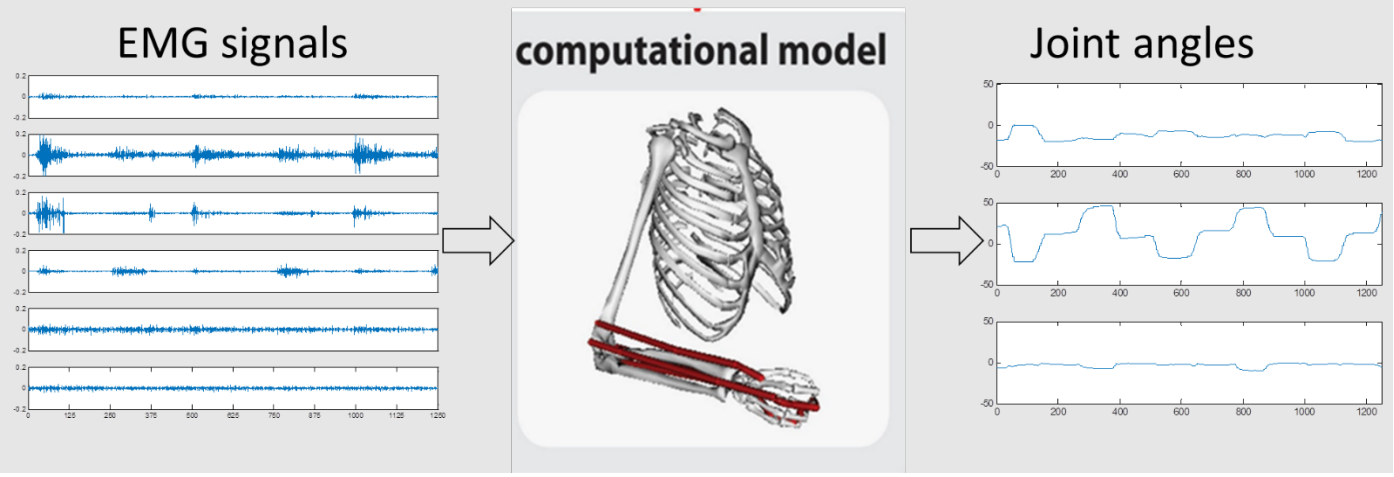

Figure 47. Block diagram of the control scheme for EMG-Driven musculoskeletal model.

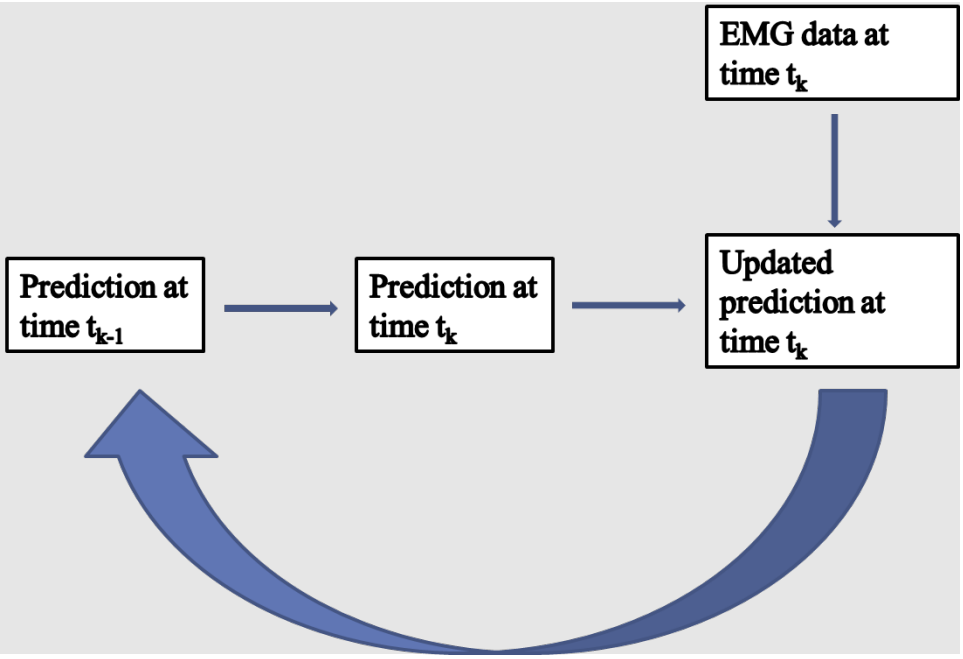

Figure 48. Block diagram of the control scheme for Kalman filter model.

Year 2

The group at NC State focused on myoelectric control and established the EMG-driven musculoskeletal model-based prosthesis control in real-time. Particularly, the following achievements have been done:

1. A musculoskeletal model for simultaneous and proportional control of 3-degrees of freedom (3-DOF) hand and wrist movements (metacarpophalangeal, MCP and wrist flexion/extension, WFLX/EXT and pronation/supination, WPRO/SUP) from EMG signals has been proposed (Figure 49).
2. The 2-DOF musculoskeletal model enabled five able-bodied subjects and a transradial amputee to control a stick-figure virtual hand in real-time to trace straight paths on a computer screen (Figure 50).
3. Evaluation of the effect of an output speed threshold method to stabilize the movement prediction of a 2-DOF musculoskeletal model-based continuous EMG controller during a real-time virtual task (Figure 51).
4. Evaluation of real-time model-based control performance during a virtual posture-matching task performed in 6 different static limb postural conditions (3 upper limb postures x 2 forearm postures). Model controlled using surface EMG electrodes. (Figure 52).
5. A prototype of the 2-DOFs wrist and 1-DoF hand mechanism was created (Figure 53) which will be used to validate the myoelectric control with low-level control. It includes 2-DOFs wrist and 1-DOF hand mechanism and control system.

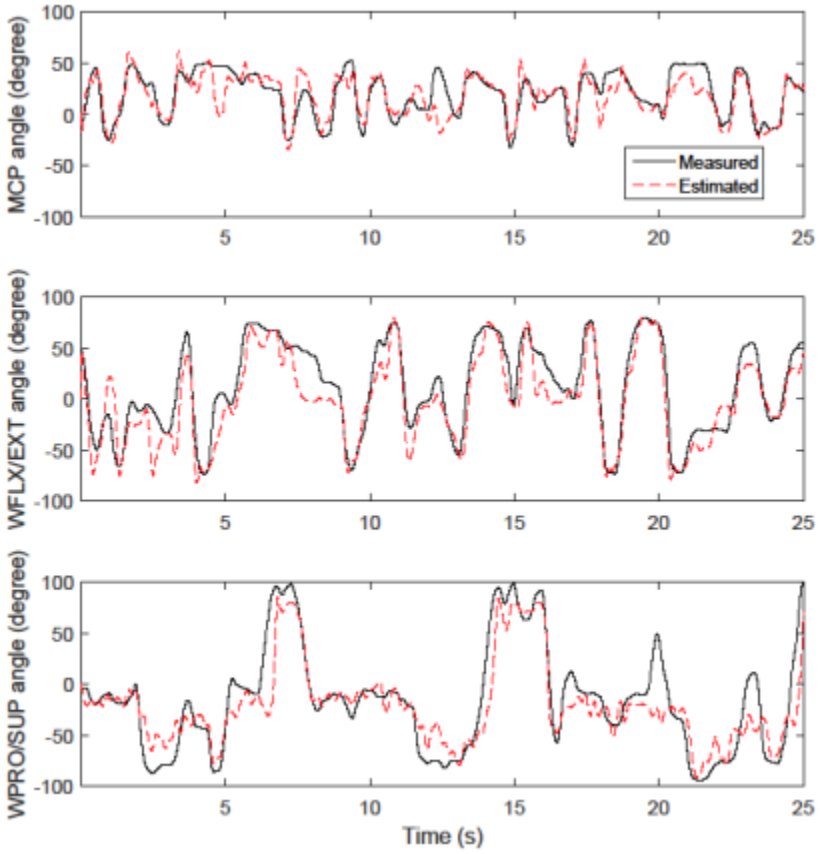

Figure 49. Measured and estimated MCP, WFLX/EXT and WPRO/SUP joint angles during simultaneous 3-DoF random movements. In this example, the correlation coefficient values for MCP, WFLX/EXT, and WPRO/SUP were 0.78, 0.93 and 0.88, respectively.

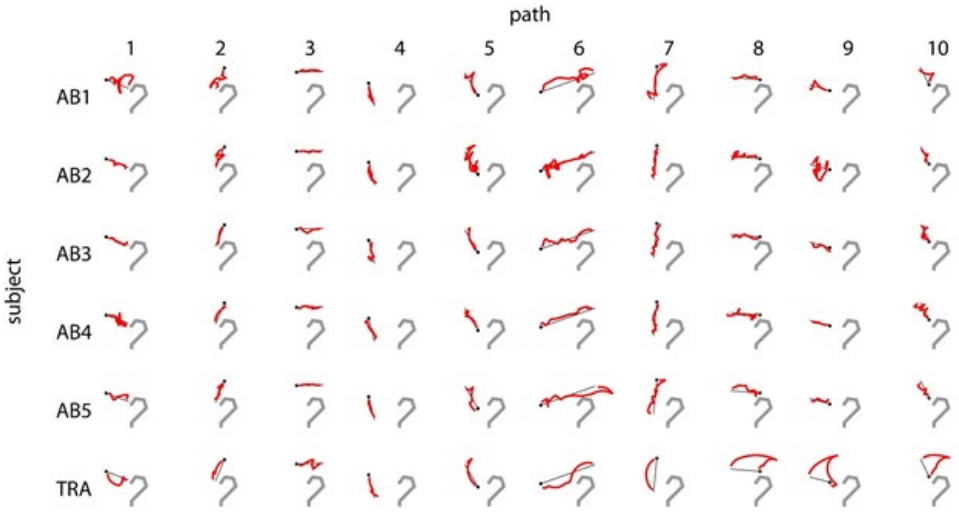

Figure 50. Fingertip trajectories (red line) from trials on day 1 testing with the lowest mean perpendicular distance. Target path (black line), start region (black dot), and virtual hand (gray line) shown for reference.

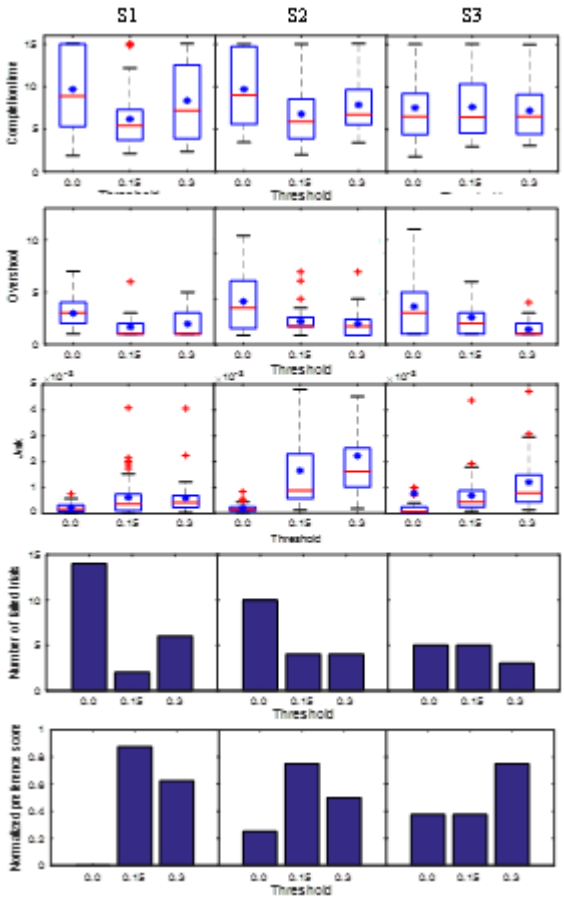

Figure 51. Performance and user preference graphs for all subjects (column order) for the 3 tested thresholds. Blue * marks show the mean on the box plots.

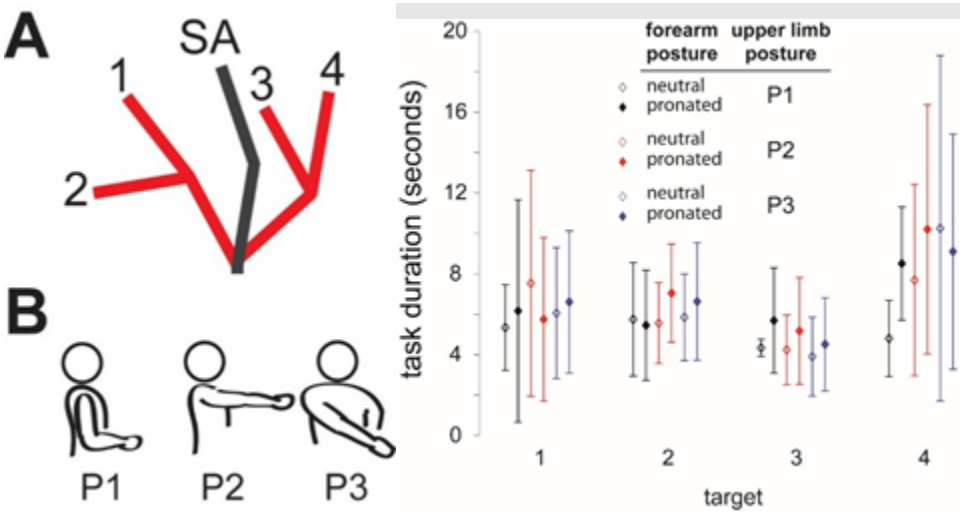

Figure 52. Task duration (in seconds) required for subjects to move from starting area (SA). A) Target positions for the MCP and wrist joints. B) Upper limb posture configurations tested. Within each arm posture, the forearm was tested in both a neutral and pronated rotated position. Task duration is shown for each target in all 6 static postural configurations (3 upper limb postures x 2 forearm postures).

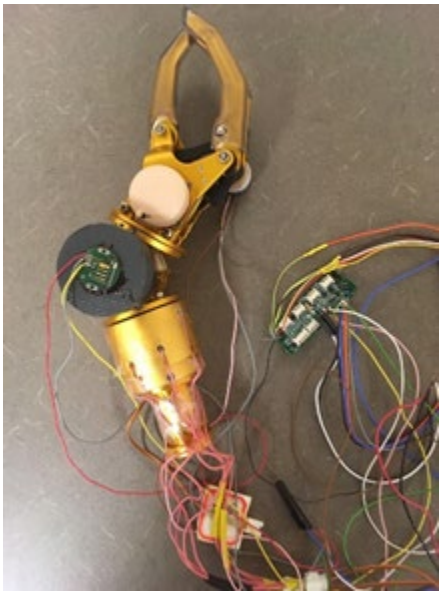

Figure 53. Prototype of the 2-DoFs wrist and 1-DoF hand system.

Year 3

The group at NC State focused on myoelectric control and established the EMG-driven musculoskeletal model-based prosthesis control in real-time. Particularly, the following achievements have been done:

1. Investigation of the effect of normalization maximum voluntary contraction electromyography (MVC-EMG) in real-time model-based control performance during a virtual posture-matching task performed in 6 different static limb postural conditions (3 upper limb postures x 2 forearm postures) (Figure 54).
2. We preliminarily tested the real-time control on the prosthetic hand with sensors for 2 of the 3 DOFs (MCP and wrist flexion/extension) on one able-bodied subject using the generic model. The subject could control the 2-DOFs of the prosthetic hand very well (Figure 55).
3. We tested the reliability of the generic model over different loading weights on eight AB subjects in this quarter. Totally, eight subjects were tested in the experiment. Subjects performed a virtual hand/wrist posture matching with three different loading weights (no weight, 1.25 Lbs, and 2.5 Lbs). (Figure 56).
4. We purchased an RIC arm with three degrees of freedom (DOFs), including hand open/close, wrist flexion/extension, and wrist pronation/supination (Figure 57), which will be used as a testing platform to validate our model-based myoelectric control with low-level control.

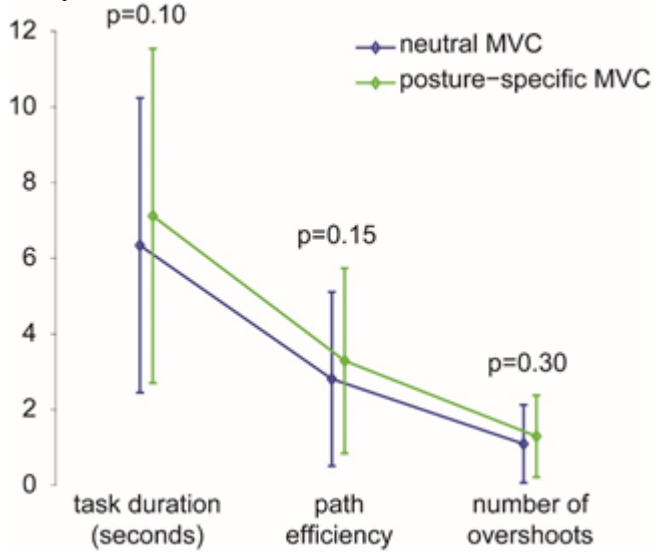

Figure 54. Task duration (seconds), path efficiency, and number of overshoots for neutral MVC and posture specific MVC.

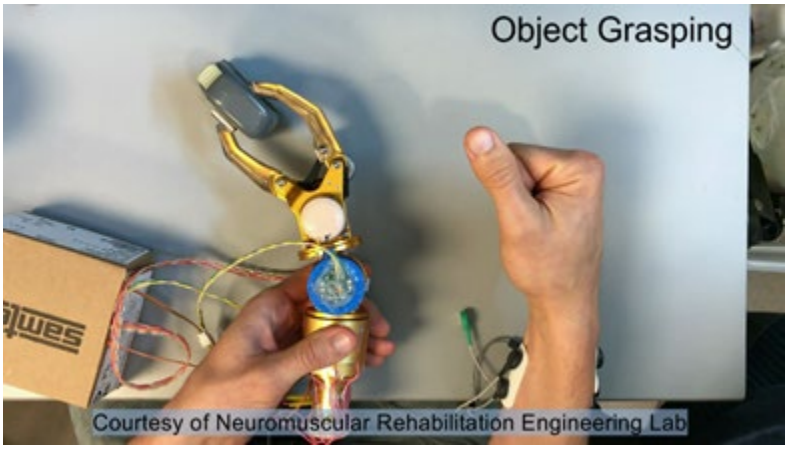

Figure. 55. Prosthetic hand real-time control on the able-bodied subject.

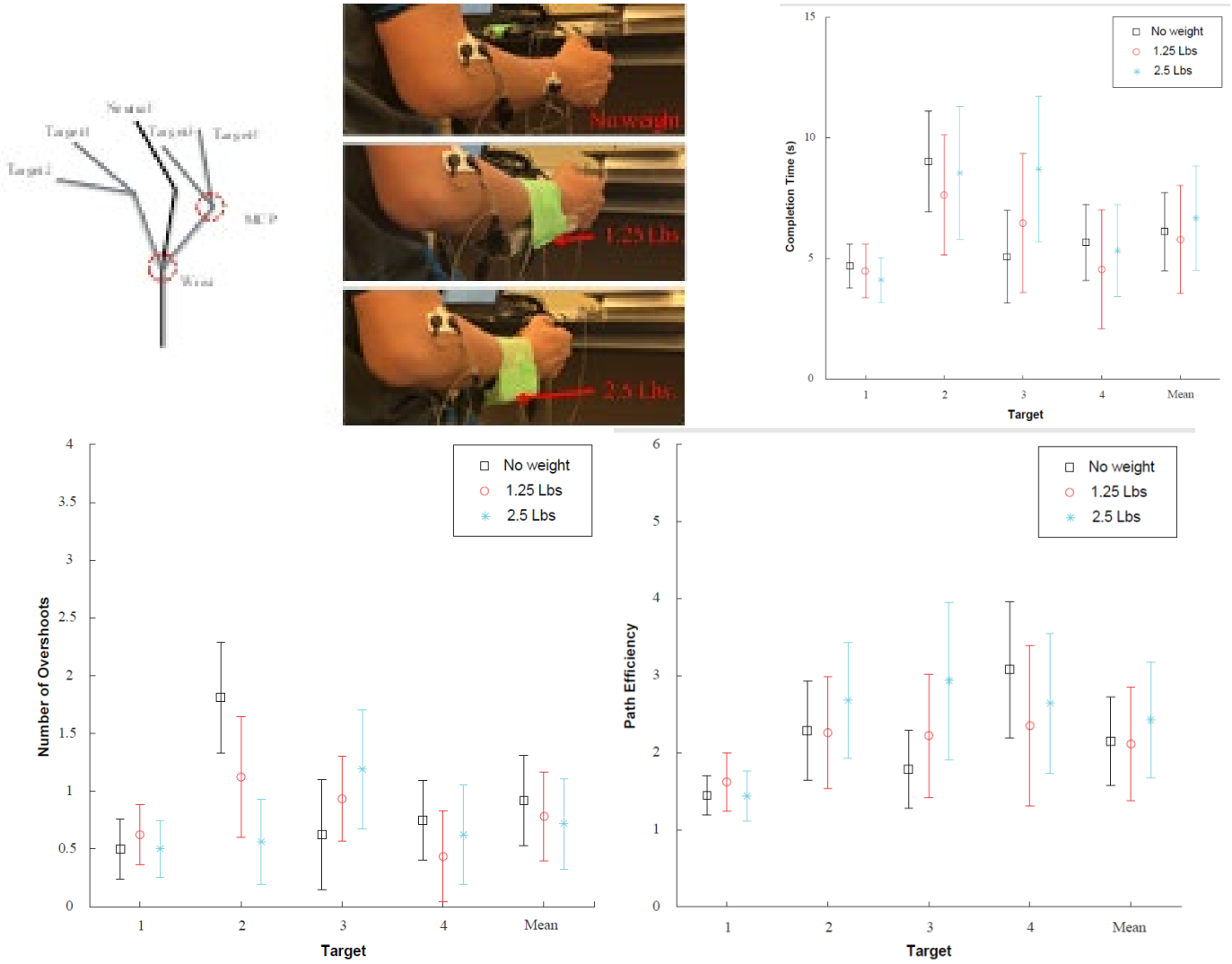

Figure 56. Average completion time, number of overshoots, and path efficiency for each target across trials for each loading weight. Error bars represent the 95% confidence interval.

Figure 57. RIC arm with three degrees of freedom (DOFs), including hand open/close, wrist flexion/extension, and wrist pronation/supination.

Year 4

The group at NC State focused on myoelectric control and established the EMG-driven musculoskeletal model-based prosthesis control in real-time. Particularly, the following achievements have been done:

1. We added joint position sensors to the 3 degrees of freedom (wrist pronation/supination, wrist flexion/extension, and hand open/close) and setup the data acquisition of these sensors to stream data to MATLAB. Two angular magnetic encoders were attached to measure hand open/close and wrist flexion extension. An off-axis rotary absolute encoder was attached measure wrist pronation/supination. The setup is shown in Figure 58.
2. We developed a PID controller, allowing for low-level, closed-loop position control of the 3 degrees of freedom (DOFs) of the RIC hand. The controller was implemented using the aforementioned sensors and data streaming in MATLAB.
3. We proposed and developed a reinforcement learning method capable of performing inverse dynamics analysis and predict the torques of the hand joints (Figure 59). This method uses surface EMG and kinematic measurements to predict the torques without external force measurements. The predicted joint moments were used to perform forward dynamics calculations to generate kinematic profiles closely matching the cross-validation datasets, as shown in Figure 60.
4. The previously mentioned reinforcement learning method was further evaluated, demonstrating fast training and the ability to generate subject-specific joint torque profiles, which is helpful in generating subject-specific musculoskeletal models. An example profile is shown in Figure 61.
5. We contacted physicians at OrthoCarolina (located in Charlotte, NC) regarding subject recruitment assistance. Following this effort, two transradial amputees have been brought in for evaluation for participation in pilot testing.

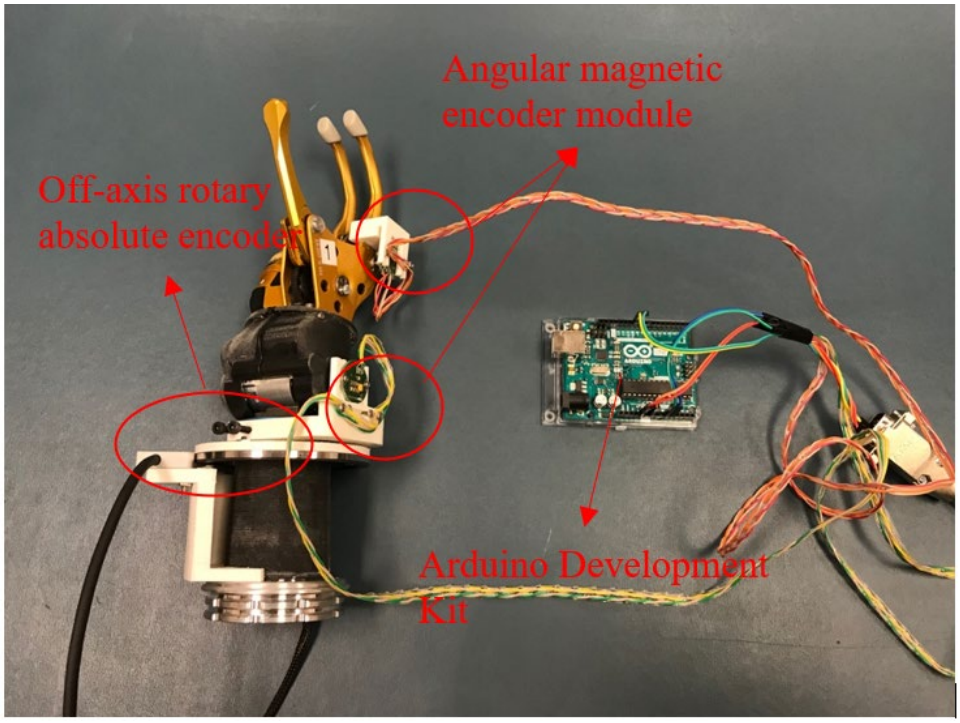

Figure 58. Three position sensors are attached to the three degrees of freedom of the RIC hand. These sensors output data to MATLAB through the Arduino Development Kit. These sensors are used in the developed PID position controller.

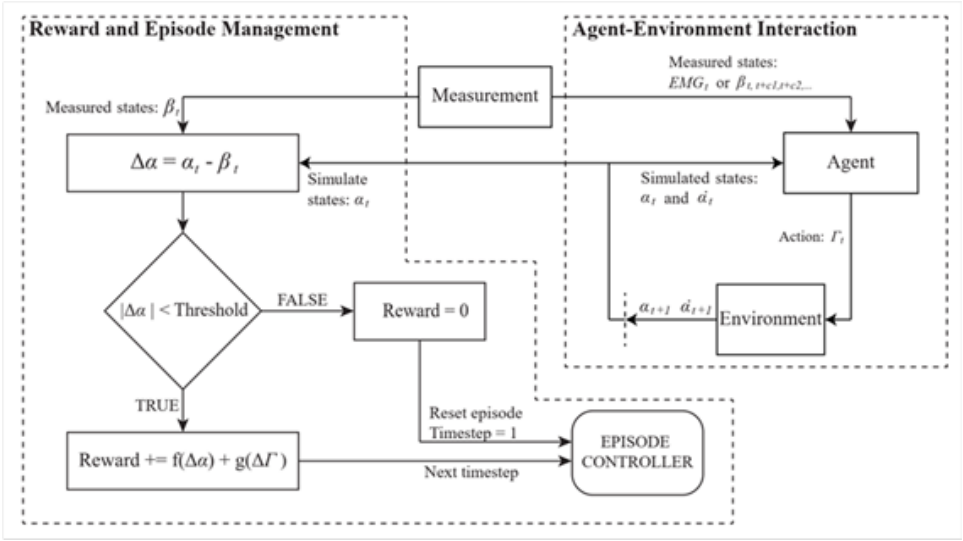

Figure 59. Block diagram outlining the reinforcement learning method for performing inverse dynamics using kinematic and surface EMG data.

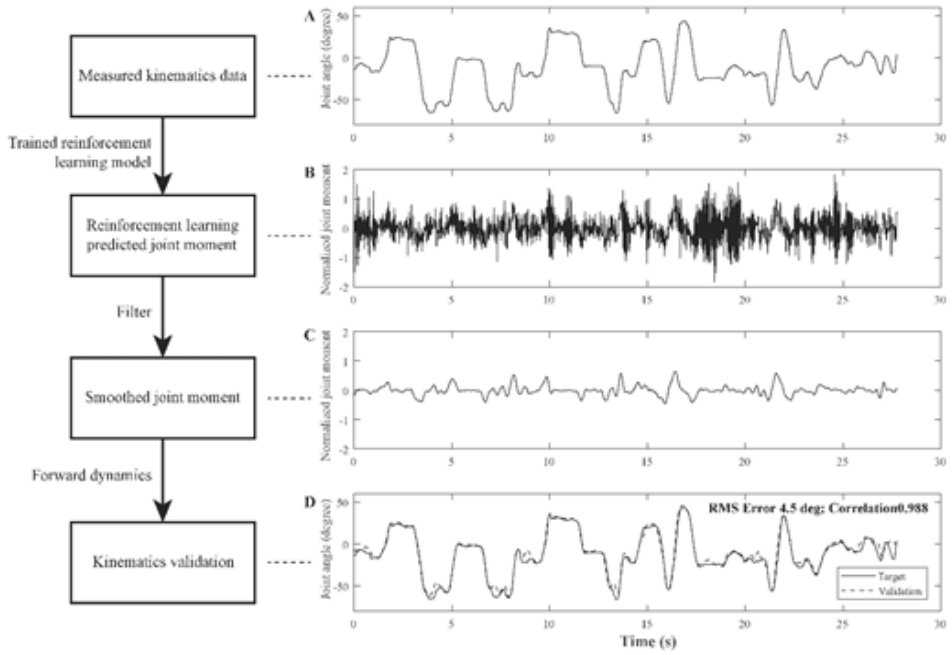

Figure 60. A diagram and example dataset of the reinforcement learning method. Kinematic data (A) are input to the trained reinforcement learning model to output joint moments (B), which are then smoothed (C) using a local regression filter. The joint moments from (C) are then used to calculate forward dynamics for validation.

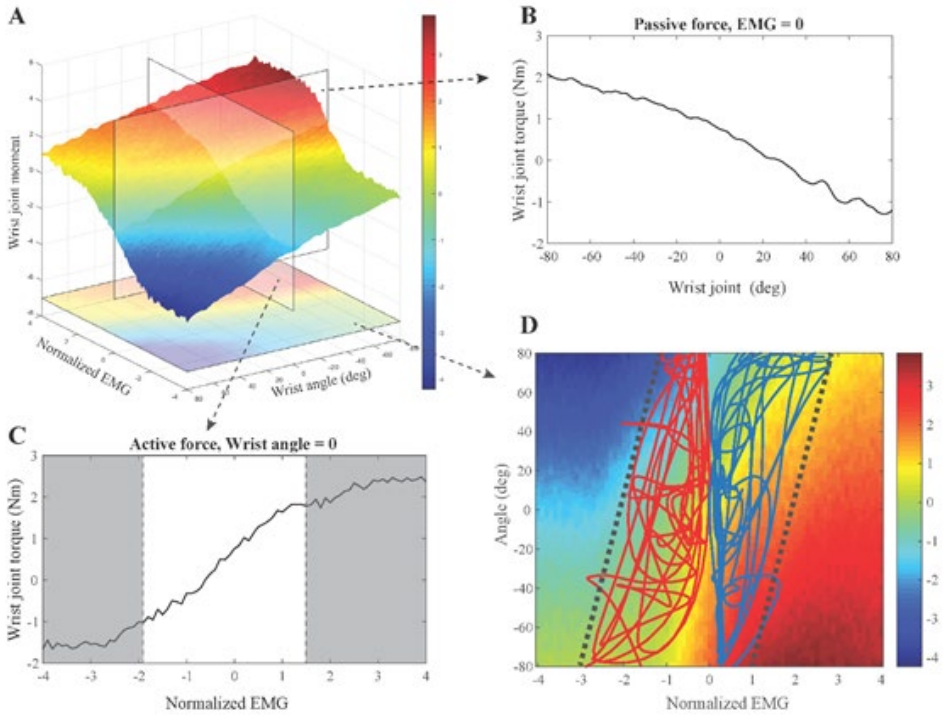

Figure 61. An example of the moment generating profile of the wrist joint for a subject as determined by the reinforcement learning method. The model determines joint moment features based on normalized EMG and joint angle (A). In (B), the joint moment as a function of joint angle, while all EMG is 0 demonstrates the passive force/moment profile. In (C), the active force/moment of the joint is shown by keeping the joint angle constant while changing muscle activity. (D) shows the dataset used to train the reinforcement learning model, with the blue curve representing the flexor EMG-wrist angle relationship and the red curve representing the extensor EMG-wrist angle relationship.

Year 5

The NCSU effort is EMG control algorithm development and implementation, as well as integrating myoelectric control with low-level control (Joint with Yale). Based on this task, the NCSU progress for this year (Sept 2019-2020) is outlined below.

1. We implemented and tuned a low-level, PID position controller for all 3 DOFs of the RIC arm. The previously added sensors were used to provide feedback and implement the controller in MATLAB. The sensors provide data to an Arduino Development Kit, which streams the data to MATLAB and controls the hand. Figure 62 shows the step response of the hand going from 10% to 90% (where 0% means close and 100% means fully open). The system is overdamped to prevent damage to the hardware from large input signals. The hand can be controlled at a rate of 50 Hz. Figure 63 shows the error signals of the PID controller over time.

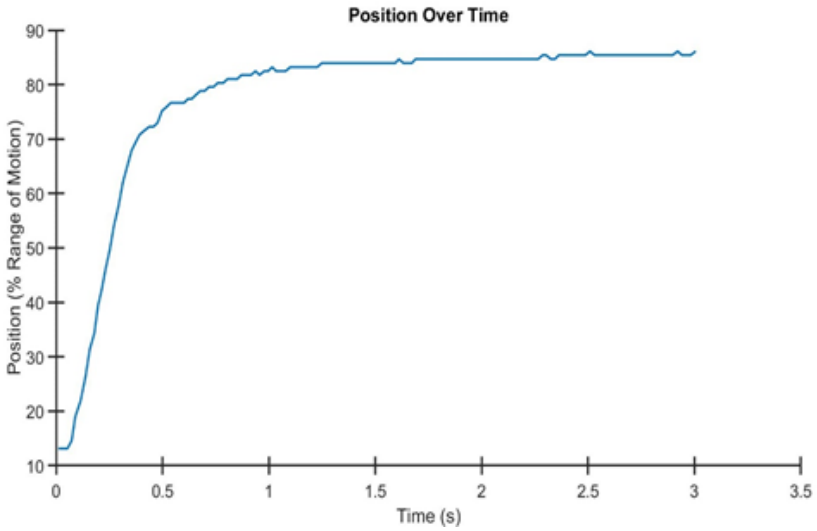

Figure 62. The hand position as a percentage of range of motion (0% being closed, 100% being fully open) over time with the PID controller. The system is overdamped to prevent damage to the hardware.

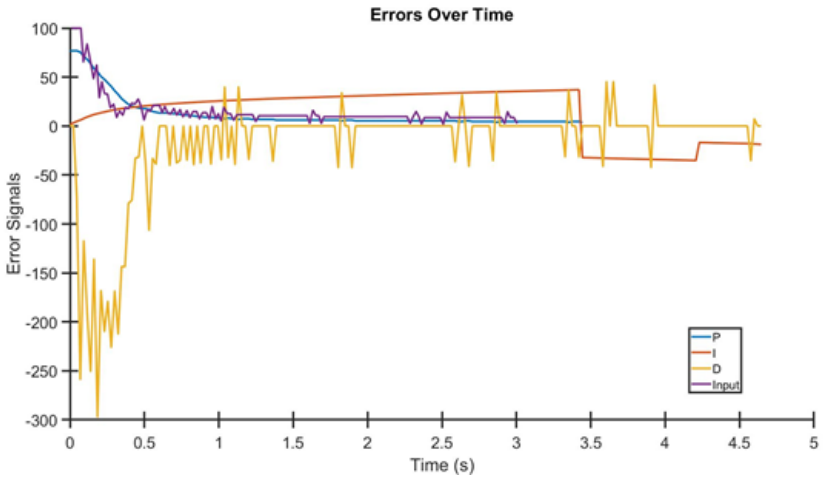

Figure 63. The error input signals of the controller. The plot shows the proportional (P), integral (I), and derivative (D) error terms as well as the resulting error signal input to the hand (Input).

2. We redesigned the 3D printed holders for the hand open/close, wrist flexion/extension, and wrist rotation joint encoders (Figure 64). This allowed for more reliable and robust measurements, allowing us to further characterize the capabilities of the robotic hand, especially with the goals of device modularity and ease-of-use in mind. The low-level PID controller was reconfigured to take advantage of the optimized sensor placements. The hand open/close reference tracking is shown as an example (Figure 65).

3. One transradial amputee subject was recruited. We collected synchronized motion capture and EMG data of finger flexion/extension and wrist flexion/extension motions. The subject performed these motions with their intact limb, which had motion capture markers on it, and attempted to mirror the motions with their

phantom limb, which had EMG electrodes on it. These data will be used to create a subject-specific musculoskeletal model controller for these two DOFs.

4. We designed and 3D printed magnetic sensor mounts with 3 DOF of adjustability, to locate the optimal sensor location, which will be used to control the wrist rotation DOF in the controls, on both an able-bodied adaptor and prosthetic socket. We tested the sensor and obtained a usable control signal from within the subject's socket (Figure 66).

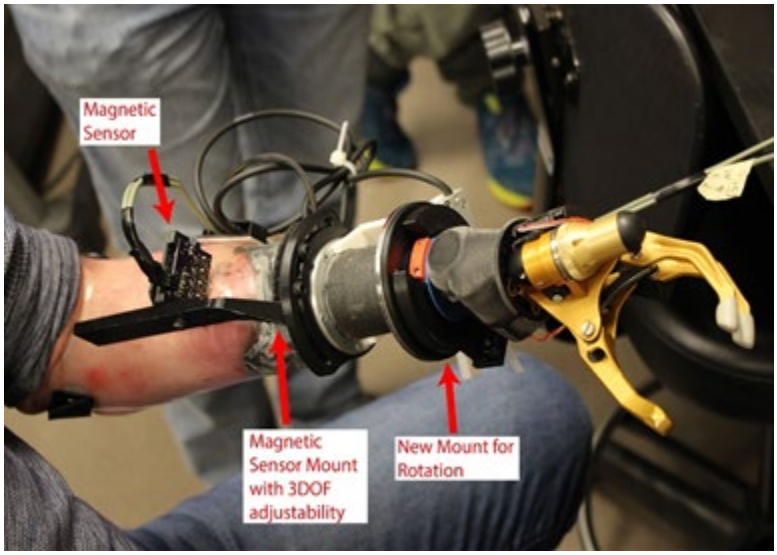

Figure 64. The robotic hand outfitted with the newly designed 3D printed encoder mounts.

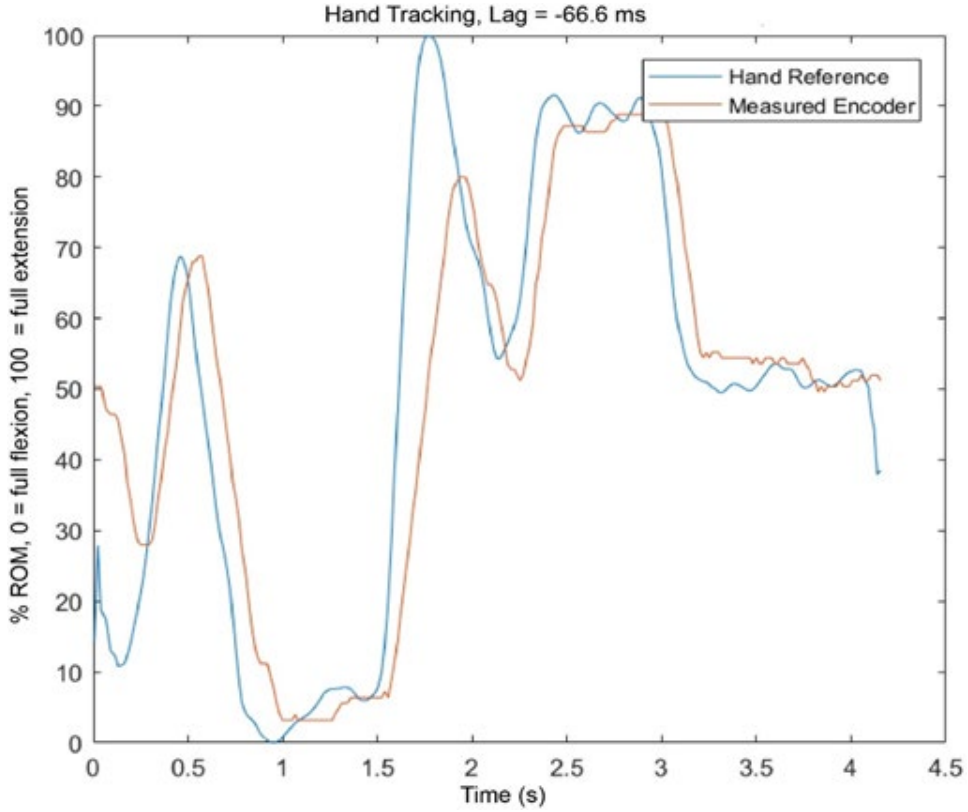

Figure 65. Hand open/close joint reference tracking. The measured joint trajectory (red line) follows the reference signal (blue line) across the entire range of motion with a lag between 60 – 70ms.

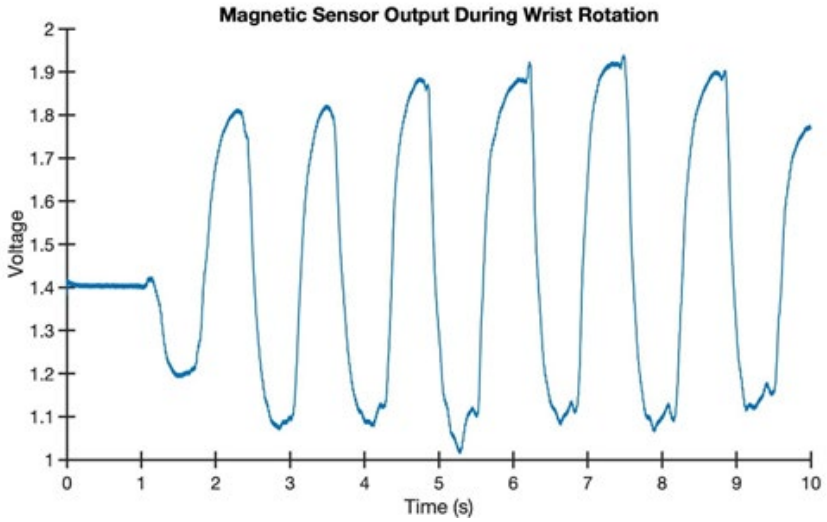

Figure 66. The output from the magnetic sensor in the amputee subject's socket during cyclic wrist pronation/supination. This sensor output will be scaled to map to physiologic wrist rotation positions.

5. **Control Scheme Development:** Previously we developed a closed loop PID position controller for all three degrees of freedom in the hand. While offline control worked successfully for pre-planned trajectories, online control has been challenging due to the limited update rate (50 Hz) of the hand purchased from the Shirley Ryan Ability Lab as noted in a prior report. To overcome this limitation, during the lab closure, we brought equipment out of the lab to improve our control scheme by introducing open-loop velocity control.
    a. To get a reliable system model, a robust characterization was performed by measuring the prosthetic hand and wrist's velocity outputs from a given motor command (Figures 67-70). Based on the identified response function, the prosthetic hand tracked the velocity outputted by the musculoskeletal model. Because the control scheme is open-loop, its performance will be evaluated when the lab is reopened where we can conduct functional tasks with an able-bodied adapter.

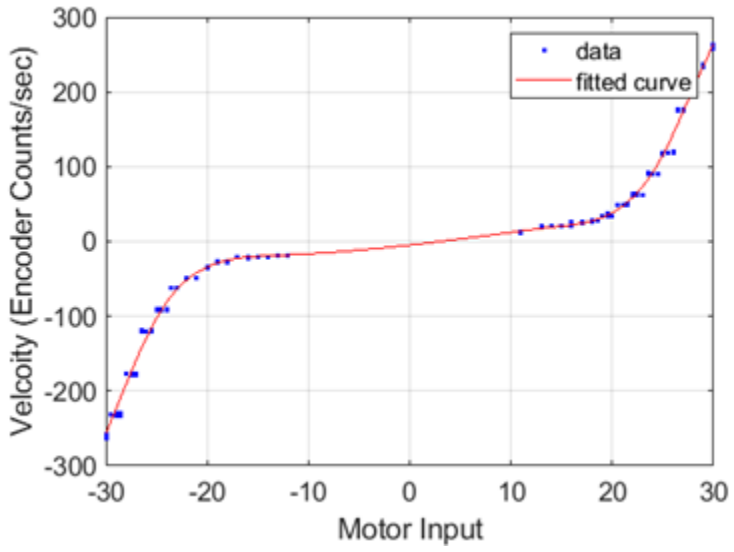

Figure 67. Open-Loop Velocity Control Characterization of the Hand. The motor saturated beyond an input of ±30. Static Friction in the hand prevented movement at motor inputs below ±10.

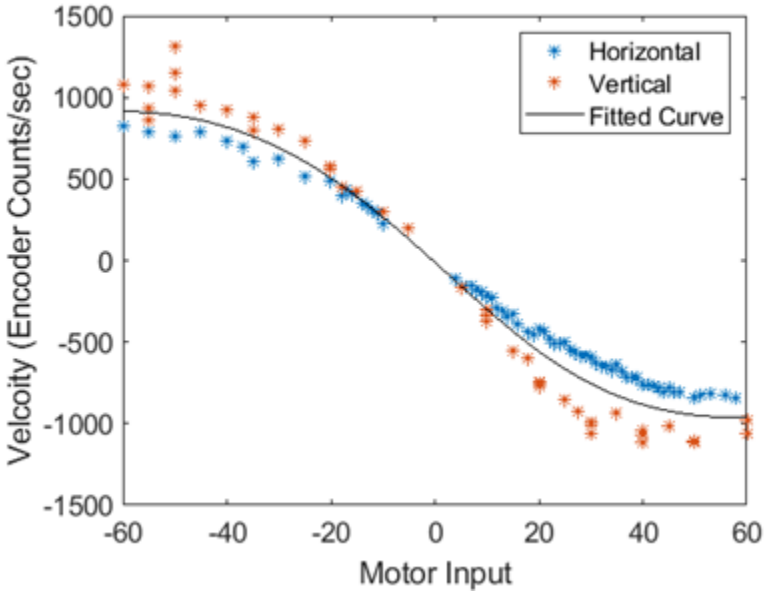

Figure 68. Open-Loop Velocity Control Characterization of the Wrist. Because of the larger moment of inertia at the wrist, robust characterization was conducted at two extremities within its workspace. The blue points indicate characterization with the wrist horizontal, parallel to the ground. In this position the hand was clutching a tennis ball to add weight and simulate a functional task (Fig. 24). The orange points indicate characterization with the wrist vertical (Fig. 25). The black line is the resulting average of the two fitted curves to account for the range in dynamics. In both cases, the motor saturated beyond an input of ±60.

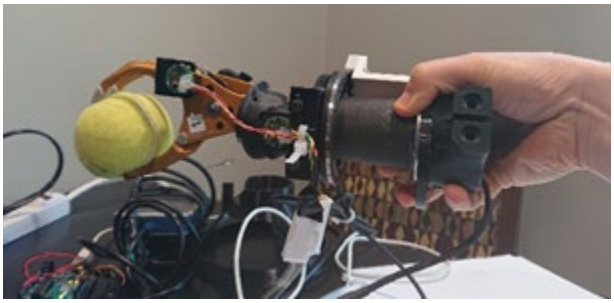

Figure 69. Wrist Characterization in Horizontal Position.

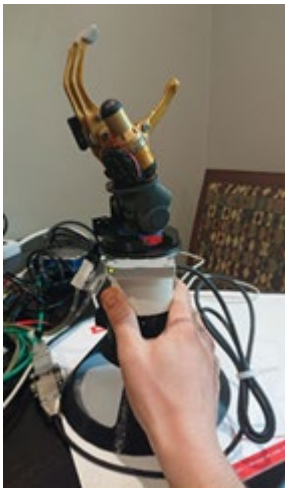

Figure 70. Wrist Characterization in Vertical Position.

6. **Additional Subject Recruitment -** During the quarantine period we were contacted by a transradial amputee who was interested in our study. After a remote screening session via Zoom, we believe they are a viable candidate for our study and plan to bring them to the lab for testing as soon as it is safe to do so.

7. **Control Scheme Implementation.** Previously we developed an open-loop velocity controller for the robotic hand by characterizing the relationship between motor inputs and resulting speeds. This controller was implemented and tested using direct myoelectric control of the hand. An able-bodied user was able to control the hand using two antagonistic muscles to drive the motors in both directions, as shown in Figure 71.

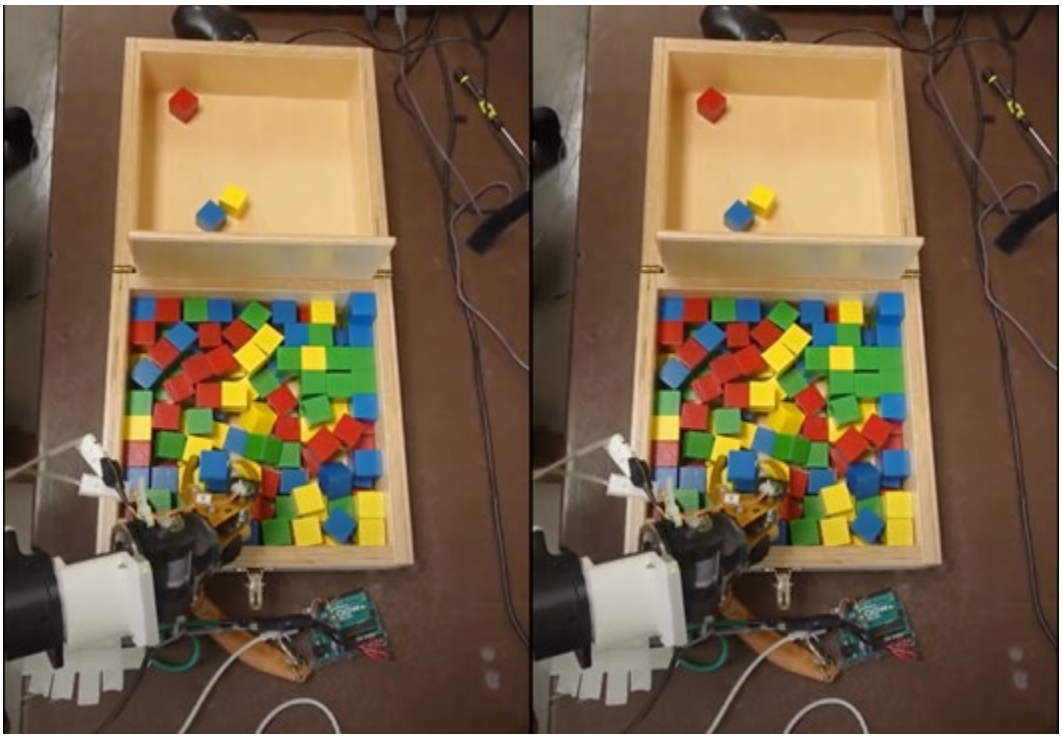

Figure 71. Open-Loop Velocity Control Implementation. An able-bodied user was able to use direct myoelectric control with the open loop control scheme to control the robotic hand to pick up blocks, transfer, and release them.

8. **Modification of the Arduino microcontroller to include CAN bus shield.** A reliable closed-loop control is critical for the musculoskeletal model based control approaches, which relies on high responding speed of the prosthetic controller. To reduce the delay of the controller, we have modified the Arduino microcontroller to include a CAN bus shield, so all low-level control schemes can be conducted on the microcontroller, eliminating communication delays between devices and allowing for better implementation of both open-loop and closed loop control. The updated setup is shown in Figure 72.

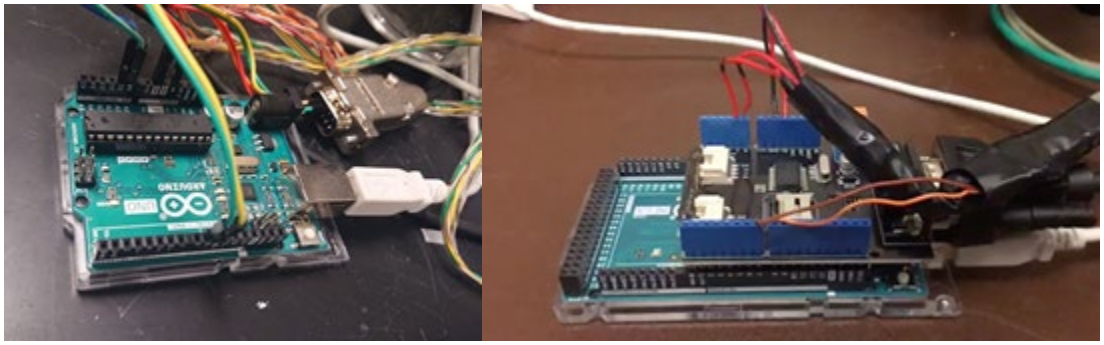

Figure 72. The previous Arduino microcontroller setup without CAN bus shield (left) compared to the modified Arduino including the CAN bus shield (right).

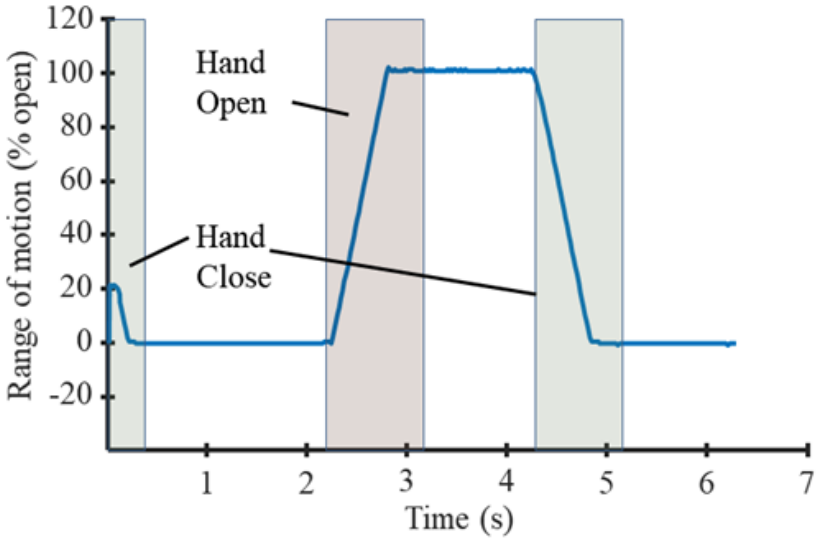

Figure 73. Validation of the controller bound checks for the hand joint. The hand position (blue line), expressed as percent of how open the hand is. Although the controller is instructed to open/close, the hand does not move out of its range of motion.

9. **Revision of Robotic Hand Safety Bounds.** Due to the limitation of adopted prosthetic hands, there exists some areas, where the joints can be stuck. To avoid these areas, we redefine the range of motion for these joints and setup virtual bounds. The effectiveness of the virtual bounds is shown in Figure 73.

10. **Pandemic Safety Protocols were Approved.** We have developed safety protocols and obtained the necessary personal protective equipment to resume testing with human subjects during the ongoing pandemic. All protocols were reviewed and approved by the IRB and Office of Research at NCSU.

3.3 What opportunities for training and professional development has the project provided?

The project members received direct training and professional development through attendance, communicating research, and networking with other researchers, at the following conferences:

- International Conference on Rehabilitation Robotics (ICORR, 2015)
- Biomedical Engineering Society Annual Meeting (BMES, 2017)
- International Conference on Biomedical Robotics and Biomechatronics (BioRob, 2018)
- American Society of Mechanical Engineer's International Design Engineering Technical Conferences (ASME IDETC) Mechanisms and Robotics Conference (2019-2020)
- International Conference on Robotics and Automation (ICRA, 2018-2019)
- Engineering in Medicine and Biology Conference (EMBC, 2020)

Additionally, the project provided opportunities to identify and examine the history and current state of the art of wrist prostheses and understand the state-of-the-art of myoelectric control for 3-DOF wrist more clearly and deeply.

3.4 How were the results disseminated to communities of interest?

The results were disseminated to communities of interest as shown in the attached conference and journal articles in the appendix.

3.5 What do you plan to do during the next reporting period to accomplish the goals?

This is the final reporting period.

4. IMPACT

4.1 What was the impact on the development of the principal discipline(s) of the project?

This project served to introduce new design ideas into the underdeveloped field of parallel mechanism wrist prostheses. Publications informed prosthesis designers of the advantages and disadvantages of parallel mechanisms versus their counterparts: serial mechanisms. Development of wrists based on parallel mechanisms have advanced, and their feasibility and advantages/disadvantages vs serial mechanism wrist designs were elaborated further. Prototypes of our wrist designs highlighted potential implementation issues. This project additionally distributed designs underactuated mechanisms into multi-grasp hand prostheses while only using a single motor. Both hardware designs aimed to show that sophistication in the hardware design can lead to successful activities of daily living by reducing fatigue (lighter devices). The project successfully introduced more advanced musculoskeletal-based models for control more intuitive for users with simultaneous control of multiple degrees of freedom based on antagonistic muscle activity. More generally, this project has identified areas in which prosthetic design may improve from nontraditional mechanism design, which is commonly not seen in currently available prosthetics on the market.

4.2 What was the impact on other disciplines?

The wrist design has several aspects of it that make it attractive in other fields, such as robotics and medical devices.

4.3 What was the impact on technology transfer?

Nothing to report.

4.4 What was the impact on society beyond science and technology?

Nothing to report.

5. CHANGES/PROBLEMS:

5.1 Changes in approach and reasons for change

The human subjects testing plan was modified – testing took place at the Yale and the NCSU study sites instead of New York. The COVID-19 Pandemic resulted in closures of the laboratory spaces and cessation of human subjects testing for multiple months at both Yale and NCSU. The spaces have since reopened at reduced capacity, and human subjects testing was modified to satisfy the health and safety regulation / suggestions put in place by the universities' IRBs and EHS, as well as to comply with state regulations.

5.2 Actual or anticipated problems or delays and actions or plans to resolve them

When constructing a physical prototype of the wrist, planned manufacturing methods may not be sufficient in construction a functional or representative prototype. For example, though we planned to 3D print portions of the wrist, we found the surface finish of the parts, or their strength may be insufficient for testing. Thus, we may have to consider more traditional, slower means of fabrication, such as machining. We received a no-cost extension for a fifth year for the project due to typical delays, mostly from prior years. Uncertainties with the COVID-19 pandemic and lockdown related issues may lead to further delay in human subjects testing. Both groups do have the capability to work on remotely on auxiliary portions of their projects if lockdowns are reinstated, but human subjects testing may be difficult / not feasible to adapt to a fully remote setting.

5.3 Changes that had a significant impact on expenditures

Nothing to report.

5.4 Significant changes in use or care of human subjects, vertebrate animals, biohazards, and/or select agents

Nothing to report.

6. PRODUCTS:

6.1 Publications, conference papers, and presentations

DL Crouch, L. Pan, H. Huang., "Musculoskeletal Model-Based Control Performance is Consistent Across Static Upper Limb Postures". 2017 BMES ANNUAL MEETING, Phoenix, AZ, 2017.

N. Bajaj and A.M. Dollar, "Kinematic Optimization of a Novel Partially Decoupled Three Degree of Freedom Hybrid Wrist Mechanism," proceedings of the 2018 IEEE International Conference on Robotics and Automation (ICRA), 2018.

L. Pan, A. Harmody, H. Huang, A Reliable Multi-User EMG Interface Based on A Generic-Musculoskeletal Model against Loading Weight Changes, Conf Proc IEEE Eng Med Biol Soc, 2018.

L. Pan, D. Crouch, H Huang*, "Myoelectric Control based on a Generic Musculoskeletal Model: Towards A Multi-User Neural-Machine Interface", IEEE Transactions on Neural System and Rehabilitation, 26(7), pp. 1435 – 1442, 2018.

N. Bajaj and A.M. Dollar, "Design and Preliminary Evaluation of a 3-DOF Powered Prosthetic Wrist Device," proceedings of the International Conference on Biomedical Robotics and Biomechatronics (BioRob), 2018.

J. Cochran, A. Spiers, and A.M. Dollar, "Analyzing At-Home Exfordance Use by Unilateral Upper-Limb Amputees," proceedings of the International Conference on Biomedical Robotics and Biomechatronics (BioRob), 2018.

M. Leddy and A.M. Dollar, "Preliminary Design and Evaluation of a Single-Actuator Anthropomorphic Prosthetic Hand with Multiple Distinct Grasp Types," proceedings of the International Conference on Biomedical Robotics and Biomechatronics (BioRob), 2018.

A. Spiers, Y. Gloumakov, and A.M. Dollar, "Examining the Impact of Wrist Mobility on Reaching Motion Compensation across a Discretely Sampled Workspace," proceedings of the International Conference on Biomedical Robotics and Biomechatronics (BioRob), 2018.

DL Crouch, L. Pan, H. Huang., Comparing Surface and Intramuscular Electromyography for Simultaneous and Proportional Control Based on a Musculoskeletal Model: A Pilot Study, IEEE Transactions on Neural System and Rehabilitation, 2018.

N. Bajaj, A. Spiers, and A.M. Dollar, "State of the Art in Artificial Wrists: A Review of Prosthetic and Robotic Wrist Design," IEEE Transactions on Robotics, vol. 35(1), pp. 261 – 277, 2019.

Y. Gloumakov, A. Spiers, and A.M. Dollar, "A Clustering Approach to Categorizing 7 Degree-of-Freedom Arm Motions during Activities of Daily Living," Proceedings of the 2019 IEEE International Conference on Robotics and Automation (ICRA), 2019.

M. Leddy and A. Dollar. "Stability Optimization of Two-Fingered Anthropomorphic Hands for Precision Grasping with a Single Actuator". The IEEE International Conference on Robotics and Automation (ICRA), Montreal, Canada, 2019.

M. Leddy and A.M. Dollar, Stability Optimization of Two-Fingered Anthropomorphic Hands for Precision Grasping with a Single Actuator," Proceedings of the 2019 IEEE International Conference on Robotics and Automation (ICRA), 2019.

N. Bajaj and A.M. Dollar, "Kinematic Optimization of a 2DOF U, 2PSS Parallel Wrist Device," Proceedings of the 2019 ASME IDETC Mechanisms and Robotics Conference, 2019.

L. Pan, D. Crouch, H. Huang*, “Comparing EMG-based human-machine interfaces for estimating continuous, coordinated movements”, IEEE Transactions on Neural System and Rehabilitation Engineering, 2019.

N. Bajaj and A.M. Dollar, “Design of a Large Workspace Passive Spherical Joint via Contact Edge Design,” Proceedings of the 2020 ASME IDETC Mechanisms and Robotics Conference, 2020.

M.T. Leddy and A.M. Dollar, “Examining the Frictional Behavior of Primitive Contact Geometries for use as Robotic Finger Pads,” IEEE Robotics and Automation Letters (with ICRA 2020 option), vol. 5(2), pp. 3137-3144, 2020.

B. Zhong, H. Huang*, E. Lobaton*, “Reliable Vision-Based Grasping Target Recognition for Upper-limb Prostheses”, IEEE Trans on Cybernetics, 2020.

J. Hong and A.M. Dollar, “A Kinematic Study of Complex Human Dexterous Manipulation Strategies: Gaiting-based Object Rotations,” proceedings of the 2020 IEEE Engineering in Medicine and Biology Conference (EMBC), 2020.

Y. Gloumakov, J. Bimbo, and A.M. Dollar, “Trajectory Control for 3 Degree of Freedom Wrist Prosthesis in Virtual Reality: A Pilot Study,” proceedings of the International Conference on Biomedical Robotics and Biomechatronics (BioRob), 2020.

Y. Gloumakov, A. Spiers, and A.M. Dollar, “Dimensionality Reduction and Motion Clustering during Activities of Daily Living: Decoupling Hand Location and Orientation,” IEEE Transactions on Neural Systems and Rehabilitation Engineering, 2020.

Y. Gloumakov, A. Spiers, and A.M. Dollar, “Dimensionality Reduction and Motion Clustering during Activities of Daily Living: 3, 4, and 7 Degree-of-Freedom Arm Movements,” IEEE Transactions on Neural Systems and Rehabilitation Engineering, 2020.

W. Wu, K Saul, He Huang* “Using reinforcement learning to estimate joint moments: An alternative solution to musculoskeletal-based biomechanics”, ASME Journal of Biomechanical Engineering, 2021

6.2 Website(s) or other Internet site(s)

Nothing to report.

6.3 Technologies or techniques

A 2-DOF wrist prototype. A custom single actuator underactuated anthropomorphic hand to be used with the wrist unit. A marker set and processing techniques associated with the motion capture system. These will accompany future publications as appendices. We have developed marker sets and processing techniques associated with the motion capture system. These will accompany future publications as appendices.

6.4 Inventions, patent applications, and/or licenses

Nothing to report.

6.5 Other Products

Nothing to report.

7. PARTICIPANTS & OTHER COLLABORATING ORGANIZATIONS

7.1 What individuals have worked on the project?

Name:	Aaron Dollar
Project Role:	PI

Researcher Identifier (e.g. ORCID ID):	Aaron.dollar@yale.edu
Nearest person month worked:	6.25
Contribution to Project:	**An expert on human hand functional use and robot / prosthetic hand development. Contributed to protocol development, measurement equipment selection, and setup.**
Funding Support:	This award.

Name:	Linda Resnik
Project Role:	Co-PI
Researcher Identifier (e.g. ORCID ID):	linda_resnik@brown.edu
Nearest person month worked:	5.2
Contribution to Project:	**An expert on upper limb prosthetics and measures of upper limb functionality and rehabilitation outcomes. Contributed to protocol development.**
Funding Support:	This award

Name:	Helen Huang
Project Role:	Co-PI
Researcher Identifier (e.g. ORCID ID):	hhuang11@NC State.edu
Nearest person month worked:	5.25
Contribution to Project:	**An expert on myoelectric control. Contributed to protocol development.**
Funding Support:	This award

Name:	Adam Spiers
Project Role:	Research Scientist
Researcher Identifier (e.g. ORCID ID):	adam.spiers@yale.edu
Nearest person month worked:	16
Contribution to Project:	**Protocol development, IRB preparation and submission, wrist technology review and publication. System overview design.**
Funding Support:	This award.

Name:	Neil Bajaj
Project Role:	Graduate Student
Researcher Identifier (e.g. ORCID ID):	neil.bajaj@yale.edu
Nearest person month worked:	60
Contribution to Project:	**Wrist technology review and publication. Wrist hardware prototype development.**
Funding Support:	This award.

Name:	Michael Leddy
Project Role:	Graduate Student
Researcher Identifier (e.g. ORCID ID):	michael.leddy@yale.edu
Nearest person month worked:	42
Contribution to Project:	**Terminal Device research, design, and evaluation**
Funding Support:	This award.

Name:	Marguerite Bowker
Project Role:	Administrative Lead

Researcher Identifier (e.g. ORCID ID):	Marguerite.Bowker@va.gov
Nearest person month worked:	1.5
Contribution to Project:	**Protocol development. IRB submissions (all institutions and DOD). Project administration.**
Funding Support:	This award

Name:	Ting Zhang
Project Role:	Postdoctoral Associate
Researcher Identifier (e.g. ORCID ID):	tzhang13@NC State.edu
Nearest person month worked:	19.75
Contribution to Project:	**Protocol development, IRB preparation, and submission,**
Funding Support:	This award

Name:	Lizhi Pan
Project Role:	Postdoctoral Associate
Researcher Identifier (e.g. ORCID ID):	lpan3@NC State.edu
Nearest person month worked:	3.75
Contribution to Project:	**Algorithm development for myoelectric control.**
Funding Support:	This award

Name:	Ming Liu
Project Role:	Postdoctoral Associate
Researcher Identifier (e.g. ORCID ID):	mliu@ncsu.edu
Nearest person month worked:	14
Contribution to Project:	**Protocol development, IRB preparation and submission,**
Funding Support:	This award

Name:	Wen Wu
Project Role:	Postdoctoral Associate
Researcher Identifier (e.g. ORCID ID):	wwu22@ncsu.edu
Nearest person month worked:	1
Contribution to Project:	**Protocol development, hardware programming, efforts related to reinforcement learning.**
Funding Support:	This award

Name:	Boxuan Zhong
Project Role:	Graduate student
Researcher Identifier (e.g. ORCID ID):	bzhong2@ncsu.edu
Nearest person month worked:	6
Contribution to Project:	**Protocol development and human subject testing**
Funding Support:	This award

Name:	Kate Barnabe
Project Role:	Administrative Lead
Researcher Identifier (e.g. ORCID ID):	Kate.Barnabe@va.gov
Nearest person month worked:	3.6
Contribution to Project:	**Protocol development. IRB submissions (all institutions and DOD). Project administration.**
Funding Support:	This award

Name:	Joao Bimbo
Project Role:	Post Doctoral Researcher
Researcher Identifier (e.g. ORCID ID):	joao.bimbo@yale.edu
Nearest person month worked:	9
Contribution to Project:	**Wrist Software and control**
Funding Support:	This award.

Name:	Yuri Gloumakov
Project Role:	Graduate Student
Researcher Identifier (e.g. ORCID ID):	yuri.gloumakov@yale.edu
Nearest person month worked:	12
Contribution to Project:	**Wrist Software and control**
Funding Support:	This award.

Name:	Rajat Singh
Project Role:	Postdoctoral Associate
Researcher Identifier (e.g. ORCID ID):	
Nearest person month worked:	12
Contribution to Project:	**Protocol development, hardware programming, efforts related to reinforcement learning.**
Funding Support:	This award

Name:	I-Chieh Lee
Project Role:	Postdoctoral Associate
Researcher Identifier (e.g. ORCID ID):	ilee5@NC State.edu
Nearest person month worked:	4
Contribution to Project:	**Algorithm development for myoelectric control**
Funding Support:	This award

Name:	Robert Hinson
Project Role:	Graduate student
Researcher Identifier (e.g. ORCID ID):	
Nearest person month worked:	7.5
Contribution to Project:	**Protocol development and human subject testing.**
Funding Support:	This award

Name:	Albert Dodson
Project Role:	Research Engineer
Researcher Identifier (e.g. ORCID ID):	
Nearest person month worked:	5.25
Contribution to Project:	**Hardware and protocol development.**
Funding Support:	This award

Name:	Joseph Berman
Project Role:	Graduate Student
Researcher Identifier (e.g. ORCID ID):	
Nearest person month worked:	2
Contribution to Project:	**Algorithm development and human subject testing.**

Funding Support:	This award

Name:	Fiona Popp
Project Role:	Graduate Student
Researcher Identifier (e.g. ORCID ID):	
Nearest person month worked:	1.5
Contribution to Project:	**Hardware development and human subject testing.**
Funding Support:	This award

7.2 Has there been a change in the active other support of the PD/PI(s) or senior/key personnel since the last reporting period?

The PI received additional funding in Year 4 from the National Science Foundation to support his robotics research, but nothing new related to rehabilitation.

7.3 What other organizations were involved as partners?

Nothing to report.

8. SPECIAL REPORTING REQUIREMENTS

A Quad Chart accompanies this report.

9. APPENDICIES

Published papers from the past year of performance are appended.

DL Crouch, L. Pan, H. Huang., "Musculoskeletal Model-Based Control Performance is Consistent Across Static Upper Limb Postures". 2017 BMES ANNUAL MEETING, Phoenix, AZ, 2017.

N. Bajaj and A.M. Dollar, “Kinematic Optimization of a Novel Partially Decoupled Three Degree of Freedom Hybrid Wrist Mechanism,” proceedings of the 2018 IEEE International Conference on Robotics and Automation (ICRA), 2018.

L. Pan, A. Harmody, H. Huang, A Reliable Multi-User EMG Interface Based on A Generic-Musculoskeletal Model against Loading Weight Changes, Conf Proc IEEE Eng Med Biol Soc, 2018.

L. Pan, D. Crouch, H Huang*, “Myoelectric Control based on a Generic Musculoskeletal Model: Towards A Multi-User Neural-Machine Interface”, IEEE Transactions on Neural System and Rehabilitation, 26(7), pp. 1435 – 1442, 2018.

N. Bajaj and A.M. Dollar, “Design and Preliminary Evaluation of a 3-DOF Powered Prosthetic Wrist Device,” proceedings of the International Conference on Biomedical Robotics and Biomechatronics (BioRob), 2018.

J. Cochran, A. Spiers, and A.M. Dollar, “Analyzing At-Home Exfordance Use by Unilateral Upper-Limb Amputees,” proceedings of the International Conference on Biomedical Robotics and Biomechatronics (BioRob), 2018.

M. Leddy and A.M. Dollar, “Preliminary Design and Evaluation of a Single-Actuator Anthropomorphic Prosthetic Hand with Multiple Distinct Grasp Types,” proceedings of the International Conference on Biomedical Robotics and Biomechatronics (BioRob), 2018.

A. Spiers, Y. Gloumakov, and A.M. Dollar, “Examining the Impact of Wrist Mobility on Reaching Motion Compensation across a Discretely Sampled Workspace,” proceedings of the International Conference on Biomedical Robotics and Biomechatronics (BioRob), 2018.

DL Crouch, L. Pan, H. Huang., Comparing Surface and Intramuscular Electromyography for Simultaneous and Proportional Control Based on a Musculoskeletal Model: A Pilot Study, IEEE Transactions on Neural System and Rehabilitation, 2018.

N. Bajaj, A. Spiers, and A.M. Dollar, "State of the Art in Artificial Wrists: A Review of Prosthetic and Robotic Wrist Design," IEEE Transactions on Robotics, vol. 35(1), pp. 261 – 277, 2019.

Y. Gloumakov, A. Spiers, and A.M. Dollar, "A Clustering Approach to Categorizing 7 Degree-of-Freedom Arm Motions during Activities of Daily Living," Proceedings of the 2019 IEEE International Conference on Robotics and Automation (ICRA), 2019.

M. Leddy and A. Dollar. "Stability Optimization of Two-Fingered Anthropomorphic Hands for Precision Grasping with a Single Actuator". The IEEE International Conference on Robotics and Automation (ICRA), Montreal, Canada, 2019.

M. Leddy and A.M. Dollar, Stability Optimization of Two-Fingered Anthropomorphic Hands for Precision Grasping with a Single Actuator," Proceedings of the 2019 IEEE International Conference on Robotics and Automation (ICRA), 2019.

N. Bajaj and A.M. Dollar, "Kinematic Optimization of a 2DOF U, 2PSS Parallel Wrist Device," Proceedings of the 2019 ASME IDETC Mechanisms and Robotics Conference, 2019.

L. Pan, D. Crouch, H. Huang*, "Comparing EMG-based human-machine interfaces for estimating continuous, coordinated movements", IEEE Transactions on Neural System and Rehabilitation Engineering, 2019.

N. Bajaj and A.M. Dollar, "Design of a Large Workspace Passive Spherical Joint via Contact Edge Design," Proceedings of the 2020 ASME IDETC Mechanisms and Robotics Conference, 2020.

M.T. Leddy and A.M. Dollar, "Examining the Frictional Behavior of Primitive Contact Geometries for use as Robotic Finger Pads," IEEE Robotics and Automation Letters (with ICRA 2020 option), vol. 5(2), pp. 3137-3144, 2020.

B. Zhong, H. Huang*, E. Lobaton*, "Reliable Vision-Based Grasping Target Recognition for Upper-limb Prostheses", IEEE Trans on Cybernetics, 2020.

J. Hong and A.M. Dollar, "A Kinematic Study of Complex Human Dexterous Manipulation Strategies: Gaiting-based Object Rotations," proceedings of the 2020 IEEE Engineering in Medicine and Biology Conference (EMBC), 2020.

Y. Gloumakov, J. Bimbo, and A.M. Dollar, "Trajectory Control for 3 Degree of Freedom Wrist Prosthesis in Virtual Reality: A Pilot Study," proceedings of the International Conference on Biomedical Robotics and Biomechatronics (BioRob), 2020.

Y. Gloumakov, A. Spiers, and A.M. Dollar, "Dimensionality Reduction and Motion Clustering during Activities of Daily Living: Decoupling Hand Location and Orientation," IEEE Transactions on Neural Systems and Rehabilitation Engineering, 2020.

Y. Gloumakov, A. Spiers, and A.M. Dollar, "Dimensionality Reduction and Motion Clustering during Activities of Daily Living: 3, 4, and 7 Degree-of-Freedom Arm Movements," IEEE Transactions on Neural Systems and Rehabilitation Engineering, 2020.

W. Wu, K Saul, He Huang* "Using reinforcement learning to estimate joint moments: An alternative solution to musculoskeletal-based biomechanics", ASME Journal of Biomechanical Engineering, 2021.